IEEE Access
Multidisciplinary ⋮ Rapid Review ⋮ Open Access Journal

Received 12 February 2024, accepted 2 April 2024, date of publication 11 April 2024, date of current version 18 April 2024.

Digital Object Identifier 10.1109/ACCESS.2024.3387748

RESEARCH ARTICLE

Hierarchical Energy Management of Hybrid Battery Storage Systems for PV Capacity Firming and Spot Market Trading Considering Degradation Costs

MARGRIT WICKE AND THILO BOCKLISCH
Chair of Energy Storage Systems, Dresden University of Technology, 01069 Dresden, Germany
Corresponding author: Margrit Wicke (margrit.wicke@tu-dresden.de)

This work was supported by the Research Project "HYBAT-Hybrid Lithium Ion Battery Storage Solution with 1500 V System Technology, Innovative Thermal Management and Optimized System Management" supported by the Federal Ministry of Economic Affairs and Climate Action under Grant 03EI3009C.

ABSTRACT Lithium-ion batteries are currently one of the key technologies for a sustainable energy transition. However, they have a limited calendar and cycle lifetime, which are directly affected by operating conditions. Therefore, our goal is to maximize the benefits of a battery storage over its entire lifespan. Stacking multiple services (multi-use) can increase the utilization of battery storage, whereas coupling different storage technologies with complementary characteristics (hybrid energy storage systems) adds a degree of freedom for efficient and degradation-aware operation. To exploit these technological and economic advantages, we develop an energy management concept and demonstrate it in the application example of a grid-connected photovoltaic plant with hybrid battery storage. The multi-use application consists of capacity firming, participation in the electricity spot market, and peak shaving. To address the different temporal scales of the battery storage tasks, we propose a hierarchical energy management with two levels. The model predictive upper level energy management optimizes the grid power considering the time-varying electricity prices and marginal costs of battery storage operation. This multi-objective optimization problem is solved using a mixed-integer linear program with two-dimensional piecewise linearization of conversion losses and battery degradation costs. The strategy-based lower level energy management allocates power in real time to meet the grid power and ramp-rate requirements despite model and forecast errors. Extensive simulations demonstrate the advantages of the proposed approach owing to a better compliance with grid power requirements, lower conversion losses, and significantly higher benefits of the battery storage system over its lifetime.

INDEX TERMS Capacity firming, degradation costs, energy arbitrage, hierarchical control, hybrid energy storage system (HESS), lithium-ion battery aging, mixed-integer linear programming (MILP), multi-use, piecewise affine (PWA) approximation, photovoltaic (PV) power integration.

ACRONYMS

BESS	Battery energy storage system
EM	Energy management
HE-BS	High-energy battery storage
HESS	Hybrid energy storage system
HP-BS	High-power battery storage
LFP	Lithium iron phosphate
LTO	Lithium titanate
MILP	Mixed-integer linear programming
PV	Photovoltaic
PWA	Piecewise affine
SOC	State of charge
SOH	State of health

The associate editor coordinating the review of this manuscript and approving it for publication was Alexander Micallef.

I. INTRODUCTION

To reduce the devastating consequences of the climate catastrophe for the Earth and the present and future generations living on it, it is necessary to move away from fossil fuels as quickly as possible [1], [2]. The use of renewable energy makes a decisive contribution to providing decent living, considering the planetary boundaries [2], [3]. A high share of volatile power generation from photovoltaic (PV) and wind plants necessitates flexibility in the energy system. Lithium-ion batteries are well suited for the mitigation of power fluctuations in the range of seconds to hours, and have seen significant technical and economic improvements over the past few years [4]. However, aging mechanisms occur in battery cells both during cycling and idle time, which limits their lifetime due to deteriorated technical performance and an increasing safety risk [5], [6]. The operating conditions of a battery energy storage system (BESS) directly affect the aging process [7]. From an economic and ecological point of view, it is therefore important to operate the BESS in a way that allows for prolonged usage with the greatest benefit possible. One concept for increasing the use of an energy storage system over its lifetime is to combine several suitable applications (multi-use), which also reduces the dependence on individual revenue streams [8], [9], [10], [11]. Furthermore, hybridization provides a way to avoid unfavorable operating conditions while meeting the same requirements. Hybrid energy storage systems (HESSs) consist of different types of energy storage with complementary characteristics, which can be leveraged through appropriate energy management (EM) to achieve higher overall efficiency, longer lifetime, and lower investment costs [10], [11], [12], [13], [14], [15]. In this study, the two concepts of multi-use and hybridization are combined.

A PV plant operating in conjunction with an HESS serves as an application example, as shown in Fig. 1. The HESS is composed of two different lithium-ion battery storages: a high-energy battery storage (HE-BS) and a high-power battery storage (HP-BS). The multi-use application of the HESS consists of three tasks:

1) Capacity firming to increase the reliability of the feed-in power and to avoid adverse effects on grid stability.
    a. Ramp-rate control: Limit the gradient of the grid power.
    b. Increased reliability: The energy exchanged with the grid should correspond to the previously defined value in each interval.
2) Trading in the spot market to match power supply and demand over time. The following two aspects can be distinguished:
    a. Energy time shift: Shifting the PV feed-in over time to take advantage of price spreads.
    b. Energy arbitrage: Temporary storage of grid electricity to exploit price spreads.
3) Peak shaving to maximize PV utilization when the grid connection capacity is limited. This can also be considered as a form of energy time shift.

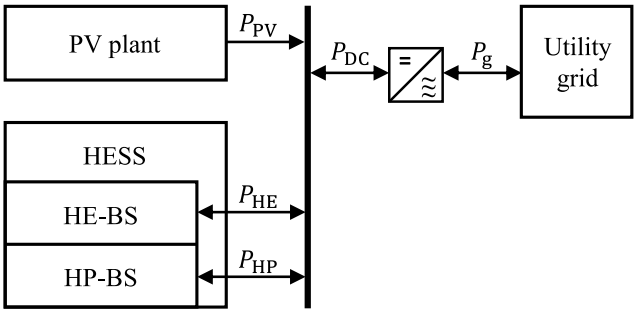

FIGURE 1. System overview.

A. LITERATURE REVIEW

PV plants are increasingly operated in conjunction with energy storage systems to meet grid code requirements or provide market-oriented services [16].

Capacity firming aims to reduce power fluctuations owing to volatile generation. A distinction can be made between smoothing or a pure ramp-rate limitation of the grid power, and capacity firming to increase reliability. In the latter case, the power of the variable renewable energy plant is usually kept constant for defined intervals, similar to a conventional generator.

Smoothing methods differ with respect to the achievable ramp-rate limitation and required energy storage capacity [17]. De La Parra et al. [18] proposed a control strategy to limit the ramp-rate of a PV energy storage system with minimum storage requirements, applying knowledge of irradiation characteristics. Several studies have promoted the use of HESSs for smoothing the feed-in power of PV and wind plants [19], [20], [21]. Hintz et al. combined a quick response and several slower response energy storage systems. The power was divided according to the states of charge (SOC) and permissible power gradients of the individual energy storage systems [19]. Jiang et al. [20] and Ma et al. [21] used an adaptive low-pass filter for smoothing. The resulting power was divided between a lithium-ion battery and a supercapacitor first via a low-pass filter and then via multi-objective optimization, considering the charge control of the supercapacitor and the total losses.

The requirement for *constant power intervals* is often derived from the participation in the energy market. Studies of HESSs have also been conducted in this regard [22], [23]. The feed-in power of a PV plant was kept constant for 15-min intervals using a lithium-ion battery and a supercapacitor in [22]. Wang et al. investigated an HESS consisting of a vanadium redox flow battery and a supercapacitor bank for dispatching a PV plant at 5-min intervals. The grid power and power allocation are determined via rule-based control [23].

Although this form of capacity firming increases the reliability of the energy exchanged with the grid, high

power gradients can occur between consecutive intervals. The conflict between a limited ramp-rate and intervals of constant power becomes more relevant, the shorter the intervals and the lower the permissible ramp-rate are. Both tendencies can be observed in electricity spot markets and grid codes [17], [24]. Therefore, we combine the two aspects of ramp-rate limitation and increased reliability of the feed-in power in our implementation of capacity firming. This approach is also used for capacity firming in French insular grids [25].

Energy time shift is another typical task of energy storage systems operated in conjunction with PV plants. Time-variable prices provide an incentive to shift feed-in from periods of low remuneration to periods of high remuneration. For example, Saez-de-Ibarra et al. used model predictive control to bid the power output of a PV plant with BESS in the day-ahead market and compensated for forecast errors via the intraday market [26]. A feed-in limit is another incentive for temporarily storing generated electricity (peak shaving on the generation side) [27].

Energy arbitrage [28], [29], [30], [31], [32], [33], in contrast, means that electricity from the grid is temporarily stored to take advantage of price differences in the electricity market. Up to now, regulatory restrictions on the subsidization of renewable energies have often stood in the way of grid supply at the same meter, but in perspective, it is a valuable addition to the multi-use portfolio. In this study, both versions, with and without grid supply, are examined.

BESS representation in the EM. When price signals determine the profitability of the BESS operation – which is especially the case in energy arbitrage – optimal control depends on marginal costs owing to power losses and degradation [34]. The aging-aware operation of BESSs is considered in an increasing number of publications, which are reviewed in [35]. An overview of the modeling of lithium-ion batteries for techno-economic analyses can be found in [36]. The literature review shows that more detailed battery models lead to a more accurate economic analysis, longer lifetime, and better compliance with the safe operating range. Gelleschus and Bocklisch demonstrated in [37] that oversimplified models in the EM of an HESS may result in drastically different system behaviors.

A conflict arises between the computational complexity of the optimization problem and real-time capability of the EM system. A common approach is to linearize the equations of the optimization problem to apply mixed-integer linear programming (MILP). Sakti et al. used piecewise affine (PWA) linearization to model the dependence of efficiency and performance constraints on battery power and SOC [28]. Xu et al. proposed a method for incorporating battery degradation costs into a MILP framework using a PWA-linearized function of cycle depth [29]. Padmanabhan et al. considered the discharge rate in addition to the cycle depth to determine degradation costs. They used multi-linear regression for linearization [30]. Hesse et al. included both efficiency and battery aging as functions of AC power in their MILP framework with PWA linearization [31]. In [29], [30], and [31], calendar aging was neglected. However, the underlying assumption that calendar aging is only negligibly affected by BESS operation should be critically examined [7]. Moreover, [32] showed that a longer calendar lifetime may be more beneficial than an extended cycle lifetime for energy arbitrage, when rare, high price spreads contribute to a significant part of the revenue. Kumtepeli et al. [33] extended the approach of [31] with a multivariate PWA linearization as a function of battery power, SOC, and temperature to represent both calendar and cyclic aging. The need for binary variables for the three-dimensional interpolation was significantly reduced by using the efficient logarithmic approach [38], [39], [40]. The authors of [33] considered the single-use case of energy arbitrage with a stand-alone BESS. In contrast, this paper investigates a BESS operated in conjunction with a PV plant for a multi-use application. Moreover, the HE-BS performance and lifetime are enhanced by hybridizing it with a HP-BS.

Hierarchical EM concepts are well suited to address the different time scales that may result from both the HESS and multi-use application. In addition, dividing the problem into several levels allows to employ the most suitable EM approach for each sub-problem [41]. Ju et al. proposed a two-level EM for a microgrid with an HESS, where the upper level EM minimizes the operation cost and the lower level EM compensates for the forecast errors [42]. A hierarchical EM concept for a microgrid with an HESS was also investigated in [43]. The EM consists of optimization-based hour-ahead scheduling and strategy-based power sharing of the HESS in one-minute resolution. Shi et al. used a two-level EM to address the different time-scales of peak shaving and fast frequency regulation [44]. This multi-use application was extended in [45] to include energy arbitrage, for which a three-level EM was developed. References [42], [43], [44], and [45] included battery aging, but neglected the calendar aging component.

B. CONTRIBUTION STATEMENT

- This article presents a robust and computationally efficient EM that comprises the two concepts of hybridization and multi-use. The HESS consists of two different lithium-ion batteries. It is deployed for PV capacity firming, energy time shift, and energy arbitrage.
- For this purpose, two levels of EM are introduced. The upper level EM is based on a state-of-the-art MILP framework with two-dimensional PWA linearization, which contains a detailed formulation of losses as well as calendar and cyclic battery aging.
- The strategy-based lower level EM draws upon the pre-optimized values and incorporates knowledge of the characteristics of solar irradiation and the two types of lithium-ion batteries for power sharing within the HESS.
- The implementation of PV capacity firming combines the aspects of ramp-rate control and increased reliability.
- Extensive simulations demonstrate the increased benefit of the BESS over its lifetime owing to the developed

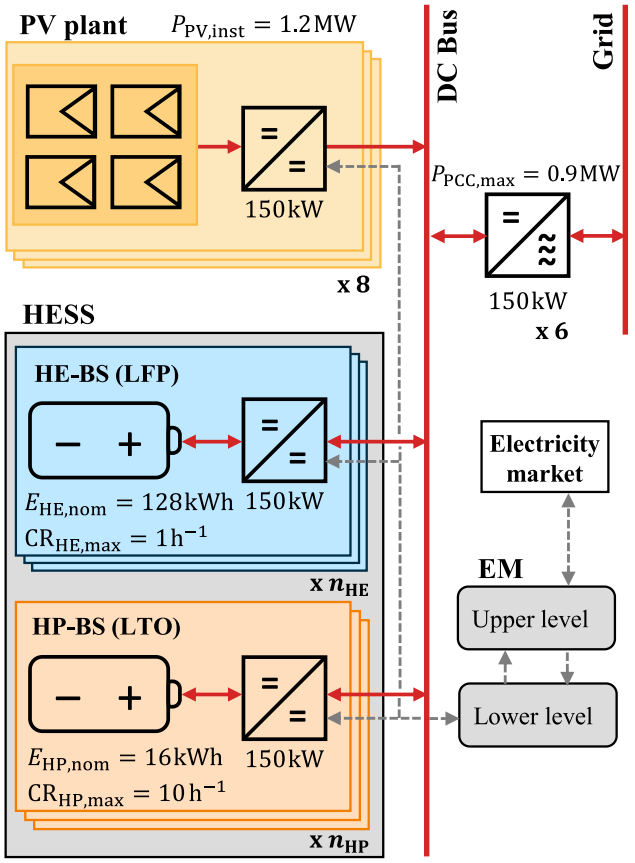

FIGURE 2. Topology of the 1.2 MW PV plant with modularized hybrid BESS. Red arrows indicate power flow and gray-dashed arrows indicate communications.

EM concept and multi-use application, as well as the advantages of HESSs from a technical and economic perspective.

The remainder of this paper is structured as follows. Section II presents the model of the PV plant with HESS and addresses battery aging. Section III delves into the hierarchical EM concept. The goals and results of the simulations are discussed in Section IV. Finally, Section V summarizes the main results and contributions of the article and provides an outlook on further investigations.

II. SYSTEM DESCRIPTION

We investigate a system consisting of a PV plant, a lithium iron phosphate (LFP) battery as the HE-BS, a lithium titanate (LTO) battery as the HP-BS, DC/DC converters, and AC/DC inverters. An overview of the system configuration is presented in Fig. 2. The PV plant has an installed power of 1.2 MW, but the maximum grid power $P_{PCC,max}$ is limited to 75 %, that is, 900 kW. To maximize the use of PV power, a DC-side coupling of the PV plant with the HESS was chosen. Each battery module is connected to the common DC bus via a bidirectional DC/DC converter. The AC/DC inverters connect the DC bus to the grid coupling point.

A. TIME SERIES

1) PV POWER PROFILE

The PV power profile was obtained from solar radiation data in one-minute resolution and the ambient temperature profile of a site in eastern Germany (Lindenberg) in 2018 [46]. For an optimal annual solar energy yield at this site, the PV modules are oriented to the south with an inclination of 38°. The power of the PV modules, P_{PVm} results from the solar radiation in the tilted plane E_{tilt}, PV module area A_{PVm}, a temperature-dependent conversion efficiency (considering the PV module efficiency η_{MPP}, temperature coefficient $\alpha_{PV,T}$, and PV module temperature T_{PVm}), and auxiliary efficiency η_{aux}, which aggregates the losses from cables, imbalances, and PV module degradation:

$$P_{PVm} = E_{tilt} \cdot A_{PVm} \cdot \eta_{MPP} \cdot (1 + \alpha_{PV,T} \cdot (T_{PVm} - 25\,°C)) \cdot \eta_{PV,aux}. \quad (1)$$

The modeling parameters are given in Table 4.

The solar radiation E_{tilt} is composed of direct and diffuse radiation in the tilted plane, as well as an additional part reflected from the ground. The direct radiation on the module plane was calculated according to [47] and the diffuse radiation was modeled using the anisotropic approach according to Perez et al. [48]. A constant standard albedo of 0.2 was assumed for the reflected radiation.

The spatial extent of a PV plant influences the short-term fluctuations in its power output. Marcos et al. [49] proposed a low-pass filter $F(s)$ as a function of plant area A_{PV} in hectares. The filter has the following transfer function:

$$F(s) = \frac{1}{(\frac{A_{PV}}{2\pi \cdot 0.02})s + 1}. \quad (2)$$

After accounting for the DC/DC conversion losses (see II-B), the theoretical annual solar energy yield is 1544 MWh.

2) PV FORECAST

The PV power profile is forecasted in 15-min mean values with a horizon of up to 24 h, and is updated every 15 min. For this purpose, we adopted the model proposed in [50]. It is based on a persistence forecast of the clear-sky factor, which describes the fracture of the actual PV energy to the theoretical PV energy under clear-sky conditions in the preceding time window. In this study, clear-sky radiation was calculated using the Metereological Radiation Model [51]. Besides the position of the sun, it requires temperature, relative humidity, atmospheric pressure and Ångström turbidity as input parameters. The former two were modeled using a simple persistence approach based on historical measurements, whereas the latter two were assumed to be constant (Table 4). A comparison of the actual PV power profile and the theoretical generation under forecasted clear-sky conditions on an example day is shown in Fig. 3. The envelopes have nearly the same shape. Exceedings of the clear-sky power profile can be explained by cloud reflections, which lead to locally increased radiation.

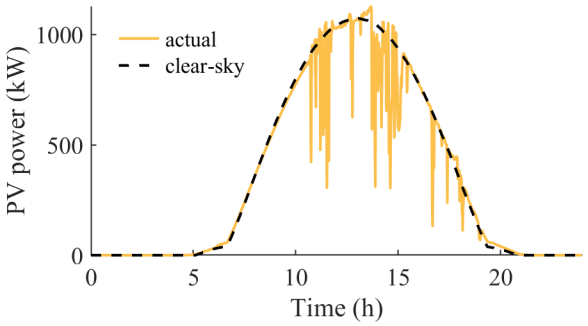

FIGURE 3. Actual PV power and theoretical power under forecasted clear-sky conditions on an example day.

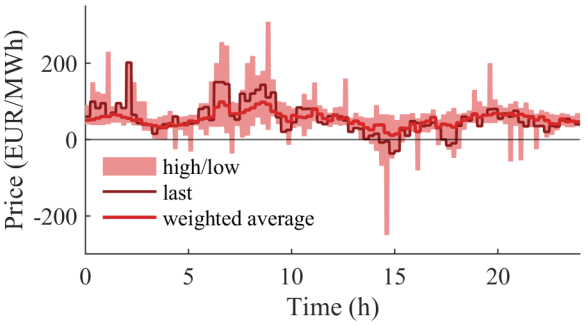

FIGURE 4. Comparison of volume-weighted average, last and high/low prices of 15-min continuous intraday market in Germany 2018 for an example day.

3) TIME-VARIABLE ENERGY PRICES AND BALANCING ENERGY

The time-varying price signal consists of historical data on intraday continuous 15-min trading in Germany in 2018 [52]. In the intraday continuous market, bid prices apply; therefore there are different prices for the same product at one trading time. This is illustrated in Fig. 4 for an example day. However, because this paper focuses on the technical investigation, the following simplifications were made: prices are fixed and known *a priori*, and the discretization of tradable power into 100-kW-steps is neglected. These simplifications are common in the literature on spot market trading with BESSs, where mostly the volume-weighted average price or the last price is used [28], [29], [31], [33].

A deviation of the average grid power from its setpoint within a quarter-hourly time interval is penalized with the payment of balancing energy. Historical data on balancing energy in Germany are publicly available [53]. In practice, revenue can be generated with the balancing energy if the individual deviation is contrary to the total deviation of the balancing group. However, this is not the point of our investigation, so all revenues due to non-fulfillment of the specified grid power are set to zero.

B. POWER ELECTRONICS

The DC/DC converters and AC/DC inverters were designed by Fraunhofer ISE within the joint research project HYBAT [54]. They have a rated power of 150 kW per module and voltage ranges of 200 V to 1500 V and 979 V to 1500 V, respectively. The loss characteristics are modeled using lookup tables. For the DC/DC converters, the dependencies of the losses on power and voltage are considered (Fig. 5a). The losses of the AC/DC inverters are assumed to be depending only on the input power (Fig. 5b). To minimize losses, the six AC/DC inverters are employed in cascades. The resulting AC/DC conversion efficiency is nearly constant.

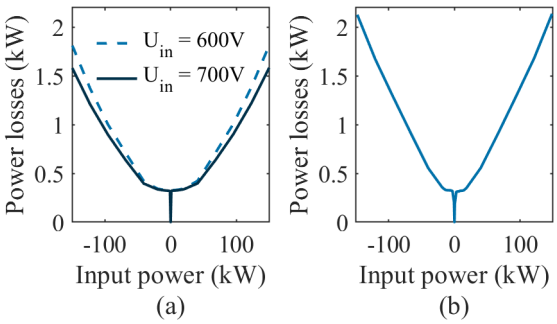

FIGURE 5. Losses of one DC/DC converter (a) and AC/DC inverter (b).

C. LITHIUM-ION BATTERIES

1) CHARGE AND LOSS CHARACTERISTICS

The HESS is composed of two different lithium-ion battery storages: an LFP battery as the HE-BS, and an LTO battery as the HP-BS. An overview of the battery module parameters is presented in Table 1. Clearly, the LFP battery has a very favorable energy-specific cost, while the LTO battery has a particularly low power-specific cost and an outstanding cycle life.

The battery modules are composed of serial and parallel connections of multiple cells, and the single-cell parameters are scaled up linearly to the module level. The basic equivalent circuit model consists of an open-circuit voltage U_{OCVm} and DC-resistance R_{im}. Both are modeled as functions of the SOC. A comparison of the open-circuit voltages and internal resistances at the module level is shown in Fig. 6. The terminal voltage U_{m} of the battery modules is calculated as a function of the battery module power P_{m}, open-circuit voltage, and DC-resistance:

$$U_{\mathrm{m}} = \frac{U_{\mathrm{OCVm}}}{2} + \sqrt{\frac{U_{\mathrm{OCVm}}^2}{4} - R_{\mathrm{im}} \cdot P_{\mathrm{m}}}. \tag{3}$$

2) LITHIUM-ION BATTERY AGING

The aging of lithium-ion batteries appears as a decrease in the usable capacity and an increase in impedance. The underlying battery aging effects can be divided into the loss of cyclable lithium, loss of active mass at both electrodes, and reduced ion mobility and electrical conductivity. These effects are based on complex aging mechanisms, including the growth of the solid electrolyte interface, lithium plating, particle cracking at both electrodes, dissolution of transition

TABLE 1. Overview of the battery module parameters.

Description	HE-BS module [55]	HP-BS module [56]
Cathode	LFP	Lithium manganese oxide/ lithium cobalt dioxide
Anode	Graphite	LTO
Cells serial	190	255
Cells parallel	2	9
Nominal energy content	128 kWh	16 kWh
Nominal capacity	210 Ah	26.1 Ah
Max. continuous C-rate	$1\,h^{-1}$	$10\,h^{-1}$
Nominal voltage	608 V	612 V
Max. voltage	693.5 V	739.5 V
Min. voltage	475 V	382.5 V
Cycle life	≈ 3500 cycles @ 25 °C, ch./dch. $1\,h^{-1}$, DOC 100 %	≈ 60000 cycles @ 25 °C, ch./dch. $10\,h^{-1}$, DOC 100 %
Assumed specific cost	230 EUR/kWh 230 EUR/kW	600 EUR/kWh 64 EUR/kW
Cost per DC/DC converter	2740 EUR	2740 EUR

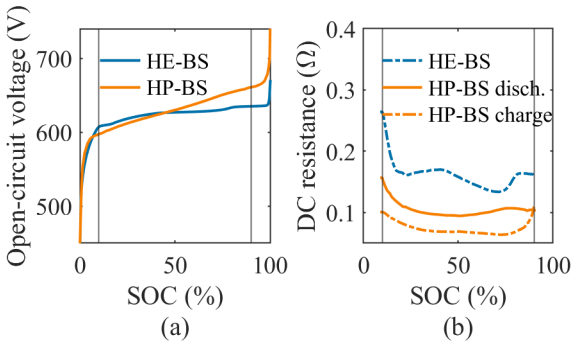

FIGURE 6. Comparison of open-circuit voltages (a) and DC-resistances (b) of the HE-BS and HP-BS modules.

metals from the positive electrode, and their structural rearrangement [5], [6]. Aging mechanisms strongly depend on the cell chemistry. A solid electrolyte interface is formed because the potential of graphite anodes lies outside the stability range of common electrolytes. Because this does not apply to LTO anodes, they do not form a solid electrolyte interface. Similarly, the high potential of LTO anodes versus Li/Li^+ largely prevents lithium plating. Volume changes in electrode materials during charge and discharge lead to particle cracking due to mechanical stress, whereas LTO anodes are a ''zero strain'' material that exhibits hardly any volume change [57]. This leads to an outstanding lifetime of LTO cells.

Various approaches exist for modeling battery aging, which can be categorized between the poles of purely theory-based and purely data-based models, and according to their accuracy and computational complexity. Semi-empirical models are typically based on small datasets obtained from accelerated aging tests. To enable a reasonable extrapolation, the models are fitted using physically informed equations. Semi-empirical models may provide acceptable accuracy with low computational effort, which makes them particularly suitable for techno-economic assessments and consideration in EM. However, the (semi-)empirically derived equations require careful statistical validation [58].

We use the semi-empirical model of an LFP cell from Naumann et al. [59], [60] to model the aging of the HE-BS. The calendar aging depends on time t, Arrhenius-law α as a function of battery temperature T_{HE}, and cubic function β of SOC_{HE}. The cyclic aging depends on the full equivalent cycles FEC_{HE}, linear function γ of C-rate CR_{HE}, and cubic function δ of the depth of cycle DOC_{HE}. The total aging in terms of capacity loss $Q_{loss}(\%)$ and increase in internal resistance $R_{inc}(\%)$ results from the superposition of calendar and cyclic aging:

$$Q_{loss} = Q_{loss,cal} + Q_{loss,cyc} \tag{4}$$

$$R_{inc} = R_{inc,cal} + R_{inc,cyc} \tag{5}$$

with

$$Q_{loss,cal} = \alpha_Q(T_{HE}) \cdot \beta_Q(SOC_{HE}) \cdot \sqrt{t} \tag{6}$$

$$R_{inc,cal} = \alpha_R(T_{HE}) \cdot \beta_R(SOC_{HE}) \cdot t \tag{7}$$

and

$$Q_{loss,cyc} = \gamma_Q(CR_{HE}) \cdot \delta_Q(DOC_{HE}) \cdot \sqrt{FEC_{HE}} \tag{8}$$

$$R_{inc,cyc} = \gamma_R(CR_{HE}) \cdot \delta_R(DOC_{HE}) \cdot FEC_{HE}. \tag{9}$$

Dynamic stress can be evaluated using the concept of ''virtual time'' and ''virtual full equivalent cycles''; the battery aging model has been verified for dynamic profiles. The model parameters can be found in [59] and [60]. In this study, we linearly scaled the cyclic aging model to match the datasheet specifications of the LFP cell (Table 1).

Since little aging is expected for the LTO cell at moderate temperatures and a continuous C-rate of $CR_{HP} \leq 10\,h^{-1}$ [56], the degradation of the HP-BS is not modeled explicitly. Instead, the HP-BS is modeled at a constant state of health (SOH) of $SOH_{HP} = 90\,\%$.

With the advanced degradation of lithium-ion batteries, a so-called aging knee can occur, from which aging accelerates. The use of the battery should usually be terminated by then, as the aging knee is not only associated with a rapid loss of capacity but also poses a safety risk. If an aging knee occurs, it often takes place around an SOH of 80 % [61], which is a typical value for the end-of-life criterion in the literature and is also used in this work.

III. ENERGY MANAGEMENT CONCEPT

The EM plays an essential role in maximizing the benefits of the HESS over its service life: The advantages of using the HESS are assessed against the disadvantages caused by battery degradation. From the plant operator's perspective, ramp-rate control and the compensation of forecast errors are mandatory, whereas monetary profit reflects the benefits of energy time shift, energy arbitrage and peak shaving. The cost of the prorated battery degradation per optimization interval is expressed monetarily as well, which is explained in III-A1. Therefore, the task of the EM is to ensure that the requirements of the applications are met, and to use the degrees of freedom to optimize the benefit-cost ratio.

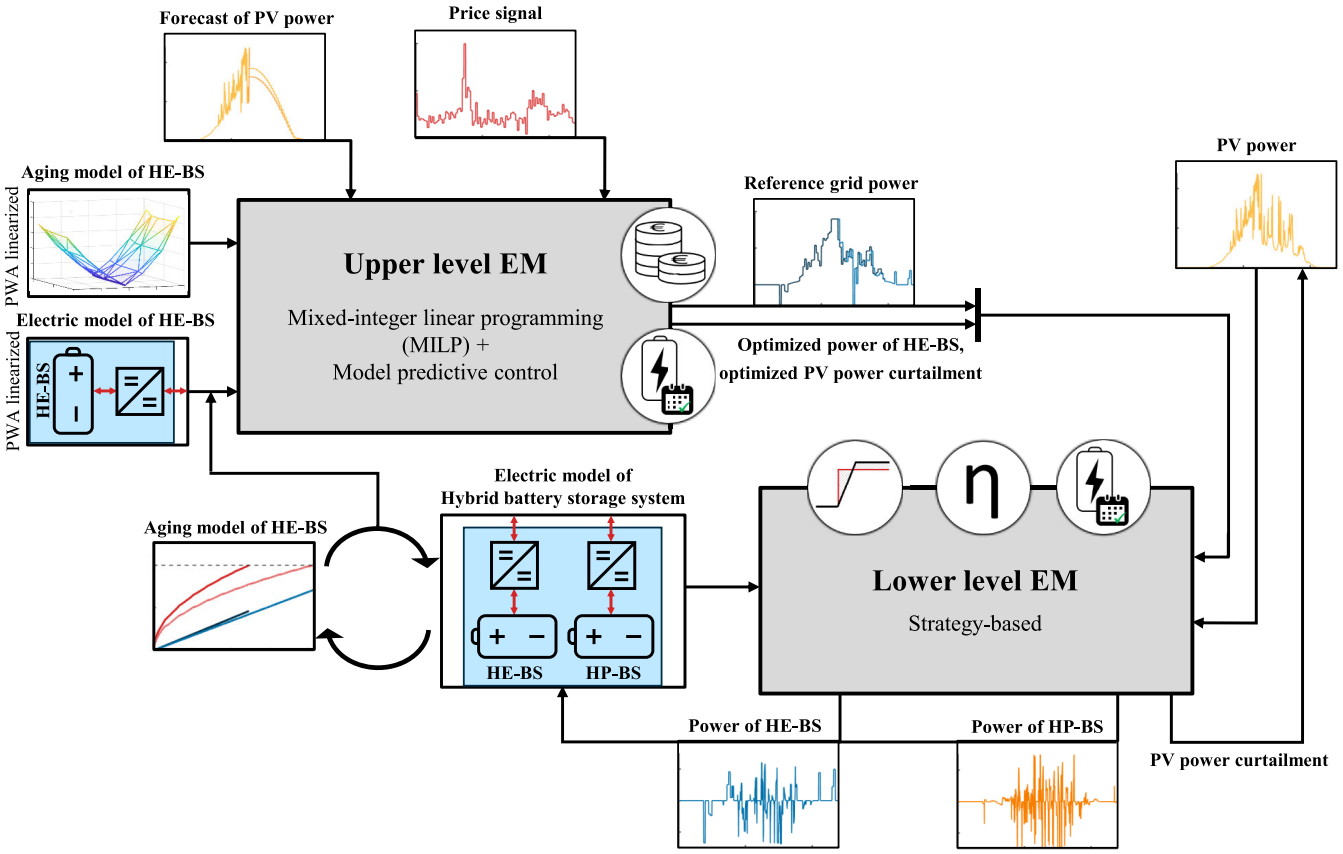

FIGURE 7. Schematic of the proposed hierarchical EM consisting of a model predictive upper level and a strategy-based lower level.

The tasks of the HESS can be located on different time scales, covering unpredicted fluctuations in the short term (up to a few minutes), to feed-in management in the medium term, to consideration of long-term battery aging phenomena. We employ a hierarchical two-level model predictive EM to address these requirements in a robust and computationally efficient manner. The EM scheme is illustrated in Fig. 7. The plant model and EM are implemented in MATLAB, and the solver Gurobi [62] is used for the optimization problem of the upper level EM.

The aim of the upper level EM is to optimize the revenues of the BESS considering degradation costs. Based on a linearized electric and battery aging model, PV forecasts, and spot market prices, the upper level EM schedules the grid power in quarter-hour intervals. Because the typical discharge time of the HP-BS is lower than the time interval $\Delta t_{\mathrm{UL}} = 15\,\mathrm{min}$ at the upper level EM, it is sufficient to consider the HE-BS at this level. The aim of the lower level EM is to meet the grid power and ramp-rate requirements despite forecast and model errors, while considering the overall efficiency and battery lifetimes. Therefore, the lower level EM first determines a grid power trajectory based on the scheduled average grid power. It then calculates the HESS power sharing using a strategy-based approach, which allows very fast response times. The model resolution and the time step of the lower level EM Δt_{LL} equal 1 min, so the subordinate control of the power converters is not within the scope of this work. An overview of how the multi-use tasks are treated at the two levels of EM is given in Table 2 and is explained in the following subsections.

A. UPPER LEVEL ENERGY MANAGEMENT

A highly nonlinear optimization problem results from the objectives of the upper level EM. However, the model predictive hierarchical EM concept allows for simplification and linearization of the optimization problem so that established and computationally efficient solvers for MILP can be used. We approximate the nonlinearities of battery aging, losses of the battery modules, and losses of the DC/DC converters with a two-dimensional PWA linearization as a function of battery power and SOC.

1) OBJECTIVE FUNCTION

The objective function (10) is composed of the spot market revenues or expenses and battery degradation costs. It includes all discrete time steps k until the end of the optimization horizon K_{MPC}. In the following, $k \in \mathbb{Z}$ and $1 \leq k \leq K_{\mathrm{MPC}}$.

Spot market revenues and expenses are calculated from the spot market price c_{spot} and the power fed into the grid P_{gf}

TABLE 2. Overview of the multi-use tasks and their handling in the two-level EM.

Task	Weighting of the task	Upper level EM	Lower level EM
Ramp-rate control	Technical requirement	Limitation of the difference between consecutive grid power reference values	Determination of a grid power trajectory with limited ramp-rate and compliance with the setpoint of energy to be exchanged with the grid
Compensation of forecast errors	Balancing energy (to be avoided)	Provision of a capacity reserve	
Energy time shift Energy arbitrage Peakshaving	Revenues/expenses at spot market vs. battery degradation costs	Optimization of grid power, power of HE-BS, and curtailment of PV power	Power sharing between the system components to comply with the determined power trajectory

or supplied by the grid P_{gs}. Grid feed-in is positive and grid supply is negative.

$$J = \min \sum_{k=1}^{K_{\mathrm{MPC}}} \Delta t_{\mathrm{UL}} \cdot \Big[-c_{\mathrm{spot}}(k) \cdot \big(P_{\mathrm{gf}}(k) + P_{\mathrm{gs}}(k)\big) + \tilde{f}_{\mathrm{degr}}(k) \cdot C_{\mathrm{b}} \Big]. \tag{10}$$

The battery degradation cost corresponds to the linearized prorated battery degradation per time step $\tilde{f}_{\mathrm{degr}}$, which is multiplied by the battery cost factor C_{b}. The derivation of $\tilde{f}_{\mathrm{degr}}$ is explained in subsection III-A2 and detailed in appendix B.

When determining the battery cost factor C_{b}, two cost components can be distinguished. First, the battery storage may generate less profit at reduced capacity and increased resistance, resulting in an opportunity cost compared to a less degraded battery storage. Second, the battery storage retires at a certain capacity loss $Q_{\mathrm{loss,EOL}} = 20\,\%$. This leads to reinvestment costs (or opportunity costs compared to the system with battery storage). Accordingly, different approaches to determine C_{b} can be found in the literature. In most cases, constant reinvestment costs are used [35]. Other approaches are simulation-based [63], [64] or based on the past added value of the battery storage for the system [65]. Collath et al. found that a simulation-based determination of the battery cost factor C_{b} provides a clear advantage if replacement of the degraded batteries is not intended [66]. As we can assume that in our use case, the battery modules are replaced when they reach their end-of-life and that this cost component dominates the degradation costs, we use constant reinvestment costs for the sake of simplicity. According to Table 1, a number of n_{HE} HE-BS modules results in

$$C_{\mathrm{b}} = 230\,\mathrm{EUR/kWh} \cdot 128\,\mathrm{kWh} \cdot n_{\mathrm{HE}}. \tag{11}$$

2) APPROXIMATION OF NONLINEARITIES

The control of the battery storage at the upper level EM is defined by the HE-BS power P_{HE}, the average $\overline{\mathrm{SOC}}_{\mathrm{HE}}$ between two time steps, and the average temperature $\overline{T}_{\mathrm{HE}}$. Because the HE-BS is located in a temperature-controlled container and operated at low C-rates, it is assumed to have a constant temperature of $T_{\mathrm{HE}} = 25\,^{\circ}\mathrm{C}$. The optimization problem contains three nonlinear functions that are dependent on both remaining variables: losses and degradation of the HE-BS modules, and DC/DC converter losses.

The HE-BS losses are represented by the overvoltage component in (3), where the open-circuit voltage is derived from the SOC. The calculation of the HE-BS current I_{HE} from P_{HE} and $\overline{\mathrm{SOC}}_{\mathrm{HE}}$ thus implicitly maps the HE-BS losses:

$$I_{\mathrm{HE}}(P_{\mathrm{HE}}, \mathrm{SOC}_{\mathrm{HE}}) = \frac{P_{\mathrm{HE}}}{U_{\mathrm{HE}}(P_{\mathrm{HE}}, \overline{\mathrm{SOC}}_{\mathrm{HE}})}. \tag{12}$$

The C-rate $\mathrm{CR}_{\mathrm{HE}}$ represents the ratio of the HE-BS current I_{HE} to the nominal HE-BS capacity $Q_{\mathrm{HE,nom}}$:

$$\mathrm{CR}_{\mathrm{HE}} = \frac{p_{\mathrm{HE}} \cdot P_{\mathrm{DC,nom}}}{U_{\mathrm{HE}} \cdot Q_{\mathrm{HE,nom}}}, \tag{13}$$

where p_{HE} is the HE-BS power normalized to the rated power of the DC/DC converters $P_{\mathrm{DC,nom}}$.

To determine the prorated battery degradation per time step, the aging model from (4) is rearranged according to the battery lifetime $t = t_{\mathrm{HE,EOL}}$ that would result under specific, constant conditions and a maximum capacity loss of $Q_{\mathrm{loss,EOL}} = 20\,\%$. Note that the global exponent in the battery aging model causes the modeled capacity loss to be independent of the order of aging stress sequences [67]. Therefore, the same degradation costs should be applied for the same aging stress regardless of the SOH.

To account for the superposition of calendar and cyclic aging, the number of full equivalent cycles must be converted into a time-dependent quantity. Under constant conditions during a sequence $\Delta\tau$, we can write

$$\mathrm{FEC}_{\mathrm{HE}} = \frac{1}{2} \cdot \mathrm{CR}_{\mathrm{HE}} \cdot \Delta\tau. \tag{14}$$

The influence of the cycle depth on the degradation is comparatively small for LFP batteries. In particular, in the middle range of the cycle depth, the employed battery aging model exhibits low sensitivity. Therefore, the cycle depth is assumed to be constant in the optimization to reduce complexity. By substituting the C-rate with (13), we obtain the bivariate degradation per time step as a function of the normalized HE-BS power and SOC:

$$f_{\mathrm{degr}} = \frac{\Delta t_{\mathrm{UL}}}{t_{\mathrm{HE,EOL}}(\overline{\mathrm{SOC}}_{\mathrm{HE}}, p_{\mathrm{HE}})} = \frac{\big[f_1(\overline{\mathrm{SOC}}_{\mathrm{HE}}) + f_2(p_{\mathrm{HE}})\big]^2}{(Q_{\mathrm{loss,EOL}})^2} \cdot \Delta t_{\mathrm{UL}}. \tag{15}$$

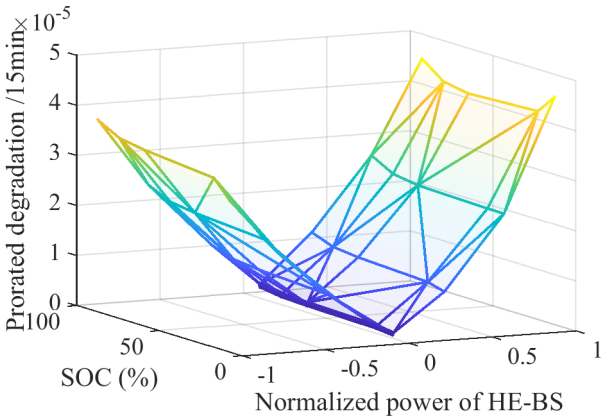

FIGURE 8. Triangulation of prorated calendar and cycle degradation of HE-BS per time interval with optimized vertices.

The losses of the DC/DC converters depend on the input power and voltage; therefore, they can also be modeled as a function of p_{HE} and $\overline{\mathrm{SOC}}_{\mathrm{HE}}$.

All three bivariate functions (C-rate, prorated degradation per time step, and losses of the DC/DC converters) are PWA linearized in two dimensions. For this, the domain of the functions is divided along the two axes into N_{p} and N_{SOC} segments. To express any point on the functions uniquely by interpolation of the vertices, the resulting rectangles must be subdivided into two triangles each [68]. For each rectangle, there are two possible subdivisions.

We used the logarithmic approach for the mathematical formulation of the PWA linearization. It is particularly suited for many segments and multidimensional functions [38], [39], [40]. A binary code, in which adjacent codewords differ by exactly one bit (Gray code) [69], is assigned to each triangle. The binary reflected Gray code is generated with a simple algorithm that can be used directly in a symmetric triangulation, such as the union-jack triangulation, in which adjacent rectangles are divided into triangles with alternating orientations (as illustrated in Fig. 13). A detailed explanation of the logarithmic formulation in the context of the EM of a BESS can be found in [33].

To minimize the computational effort of the optimization problem, we use the same vertices for all the three functions. The HE-BS power p_{HE} is divided into eight segments and the $\overline{\mathrm{SOC}}_{\mathrm{HE}}$ into four segments. This results in 64 triangles, which corresponds to six binary variables per time step in the formulation of the optimization problem. We adapted the h-hop-constrained shortest path method from [70] to multicriterially optimize the positions of the vertices for all three functions. The linearization errors of the C-rate, prorated degradation per time step, and losses of the DC/DC converters were weighted with 0.3, 0.4 and 0.3, respectively, using the sum of squared deviations as the error metric. The algorithm additionally returns the orientation of the union-jack triangulation. The resulting triangulation of the prorated battery degradation per time step is shown in Fig. 8. The vertices around $p_{\mathrm{HE}} = 0$ are close to each other, because here the curvatures of the battery degradation costs and DC/DC converter losses are particularly high.

Appendix B illustrates the workflow for two-dimensional PWA linearization using the logarithmic approach with union-jack triangulation, and provides the equations for the MILP formulation.

3) FURTHER OPTIMIZATION PROBLEM CONSTRAINTS

This subsection introduces further constraints on the optimization problem. The power balance is established at the common DC bus. A constant efficiency η_{DCAC} is assumed for the AC/DC inverters. Therefore, a distinction is made between the grid feed-in power P_{gf} and grid supply power P_{gs}. The losses of the DC/DC converters are denoted by $P_{\mathrm{DC,L}}$. The power balance is:

$$\frac{1}{\eta_{\mathrm{DCAC}}} \cdot P_{\mathrm{gf}}(k) + \eta_{\mathrm{DCAC}} \cdot P_{\mathrm{gs}}(k) - P_{\mathrm{HE}}(k) + P_{\mathrm{DC,L}}(k) + P_{\mathrm{ct}}(k) = \hat{P}_{\mathrm{PV}}(k). \tag{16}$$

$\hat{P}_{\mathrm{PV}}$ is the forecasted PV power and P_{ct} is the PV power curtailment. The power balance variables are limited as follows:

$$P_{\mathrm{HE,ch,max}} \leq P_{\mathrm{HE}}(k) \leq P_{\mathrm{HE,dch,max}} \tag{17}$$

$$0 \leq P_{\mathrm{ct}}(k) \leq \hat{P}_{\mathrm{PV}}(k) \tag{18}$$

$$0 \leq P_{\mathrm{DC,L}}(k) \leq P_{\mathrm{DC,L,max}}, \tag{19}$$

where battery charging power is negative. $P_{\mathrm{HE,ch,max}}$ and $P_{\mathrm{HE,dch,max}}$ are the maximum charging and discharging powers of the HE-BS, respectively. The binary variable $u \in \{0, 1\}$ prevents simultaneous grid feed-in and supply:

$$0 \leq P_{\mathrm{gf}}(k) \leq P_{\mathrm{PCC,max}} \cdot u(k) \tag{20}$$

$$0 \leq -P_{\mathrm{gs}}(k) \leq P_{\mathrm{PCC,max}} \cdot (1 - u(k)). \tag{21}$$

When charging the BESS from the grid is not allowed, the grid supply power P_{gs} and the binary variable u are omitted. The SOC balance is

$$\mathrm{SOC}_{\mathrm{HE}}(k+1) = \mathrm{SOC}_{\mathrm{HE}}(k) - \Delta t_{\mathrm{UL}} \cdot \frac{\mathrm{CR}_{\mathrm{HE}}(k)}{\mathrm{SOH}_{\mathrm{HE}}}, \tag{22}$$

where $\mathrm{SOH}_{\mathrm{HE}}$ represents battery aging as a function of capacity loss:

$$\mathrm{SOH}_{\mathrm{HE}} = 1 - \frac{Q_{\mathrm{HE,loss}}}{Q_{\mathrm{HE,nom}}}. \tag{23}$$

The SOH is updated every two days and therefore remains constant within the optimization horizon. The C-rate and SOC range of the HE-BS are given by:

$$\mathrm{CR}_{\mathrm{HE,min}} \leq \mathrm{CR}_{\mathrm{HE}}(k) \leq \mathrm{CR}_{\mathrm{HE,max}} \tag{24}$$

$$\mathrm{SOC}_{\mathrm{HE,min,UL}}(k) \leq \mathrm{SOC}_{\mathrm{HE}}(k) \leq \mathrm{SOC}_{\mathrm{HE,max}}. \tag{25}$$

The time-dependent parameter $\mathrm{SOC}_{\mathrm{HE,min,UL}}(k)$ is higher than the actual $\mathrm{SOC}_{\mathrm{HE,min}}$ during daytime. This allows the HE-BS to contribute to the compensation of PV power forecast errors when the available energy of the HP-BS is insufficient. A hard limit on the SOC range is implemented in

the lower level EM. If the SOC falls below $\mathrm{SOC}_{\mathrm{HE,min,UL}}(k)$, a constraint to recharge is activated in the upper level EM.

Furthermore, the difference between consecutive grid power reference values is limited to ensure that capacity firming requirements can be met. This is explained in the following subsection.

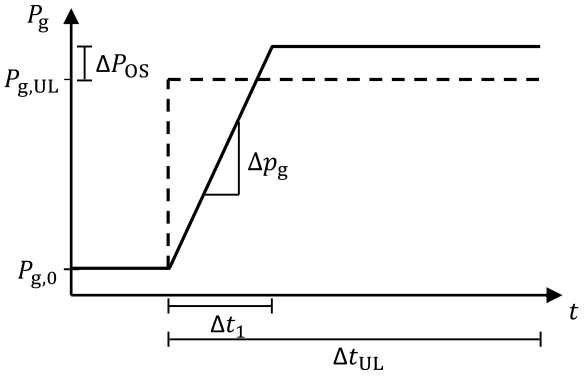

FIGURE 9. Calculation of the grid power trajectory for an average reference power $P_{g,UL}$ and a constrained ramp-rate Δp_g.

B. LOWER LEVEL ENERGY MANAGEMENT

1) DETERMINATION OF THE GRID POWER TRAJECTORY

The first task of the lower level EM is to determine a grid power trajectory P_g from the reference power $P_{g,UL}$ which was settled by the upper level EM. Since only the average power values per quarter-hour interval are evaluated in the spot market, the grid power trajectory is designed to equal the reference power in its mean value and to be bounded in its gradient. This approach links the two aspects of capacity firming: increased reliability of renewable power generation and ramp-rate limitation. The trajectory consists of two parts, as shown in Fig. 9 for a power increase. Here, the initial grid power is P_{g0} and the average reference power for the next time interval is $P_{g,UL}$. In the first segment of the trajectory, the grid power increases or decreases linearly with gradient Δp_g, which is relative to the maximum grid power $P_{PCC,max}$. In this study, the grid power gradient is limited to $\Delta p_{g,max} = 20\,\%/\mathrm{min}$. The first segment of the trajectory has a duration of Δt_1, which is calculated according to (26). This results in the first constraint of the power difference in (27).

$$\Delta t_1 = \Delta t_{UL} \cdot \left(1 - \sqrt{1 - \frac{2}{\Delta p_g \cdot \Delta t_{UL}} \cdot |(P_{g,UL} - P_{g0})|}\right) \tag{26}$$

$$|(P_{gf} + P_{gs} - P_{g0})| \leq \frac{\Delta p_g \cdot \Delta t_{UL}}{2} \tag{27}$$

The second segment of the trajectory has a constant power value with an overshoot ΔP_{OS} over the average reference power. It must be ensured that the overshoot does not violate any constraints such as the maximum allowable battery or grid power. For the configuration considered in this study, this concerns the maximum battery charging power $P_{ch,max}$ at negative gradients in (28) and the maximum grid feed-in power $P_{PCC,max}$ at positive gradients in (29):

$$P_{gf} + P_{gs} \geq P_{ch,max} + \frac{(P_{ch,max} - P_0)^2}{2 \cdot p_{rr} \cdot \Delta t} \tag{28}$$

$$P_{gf} + P_{gs} \leq P_{PCC,max} - \frac{(P_{PCC,max} - P_0)^2}{2 \cdot p_{rr} \cdot \Delta t}. \tag{29}$$

Constraints (27) – (29) are implemented in the upper level EM. Because they are convex, they can easily be replaced by several linear constraints.

Finally, the required power of the HESS $P_{HESS,ref}$ results from the grid power trajectory and the actual PV power.

2) CALCULATION OF HESS POWER SHARING

The second task of the lower level EM is to share the required power $P_{HESS,ref}$ between the HE-BS and HP-BS. The aim of HESS power sharing is to leverage the advantageous properties of each storage technology. For real-time power sharing, mainly rule-based and filter-based methods are used [10]. As presented in II-C, the LTO HP-BS has a high power capability, low losses, and a particularly long cycle life. The LFP HE-BS has a high energy density and low investment cost. This corresponds to typical complementary properties of HESSs. On the other hand, the differences in the absolute maximum power of the HE-BS and HP-BS and the losses that occur are comparatively small. Another typical property of the high-energy storage in an HESS is that a reduction in its power dynamics leads to an extended lifetime, which is not *per se* the case for lithium-ion batteries [7], [72]. Therefore, the combination of two different lithium-ion batteries can be considered as a special case of an HESS, and the advantages of a filter-based method only apply to a limited extent. For this reason, we developed a distinct strategy for the lower level EM, as illustrated in Fig. 10.

In the first step, the HE-BS is allocated no more than the pre-optimized power $P_{HE,UL}$ (blue block in Fig. 10). The resulting power $P^*_{HE,ref}$ can be further reduced to adjust the SOC of the HP-BS (yellow block). This means that the charge control of the HP-BS is only applied to the extent that it does not result in greater stress on the HE-BS. Only if the HP-BS cannot cover the residual power $P_{HP,ref}$, the HE-BS takes over a higher power than pre-optimized (red block in Fig. 10). It is further important to consider the possible curtailment of PV power because the storage of excess PV power is already optimized considering degradation in the upper level EM – yet based on an error-prone PV power forecast. This error is circumvented by limiting the charging power of the HE-BS to the optimized value $P_{HE,UL}$ in the case of a predicted curtailment of PV power ($P_{ct,UL} > 0$).

Charge control of the high-power energy storage is a central task in the EM of HESSs. The first step is to determine the reference SOC $\mathrm{SOC}_{HP,ref}$. Usually, a constant value is

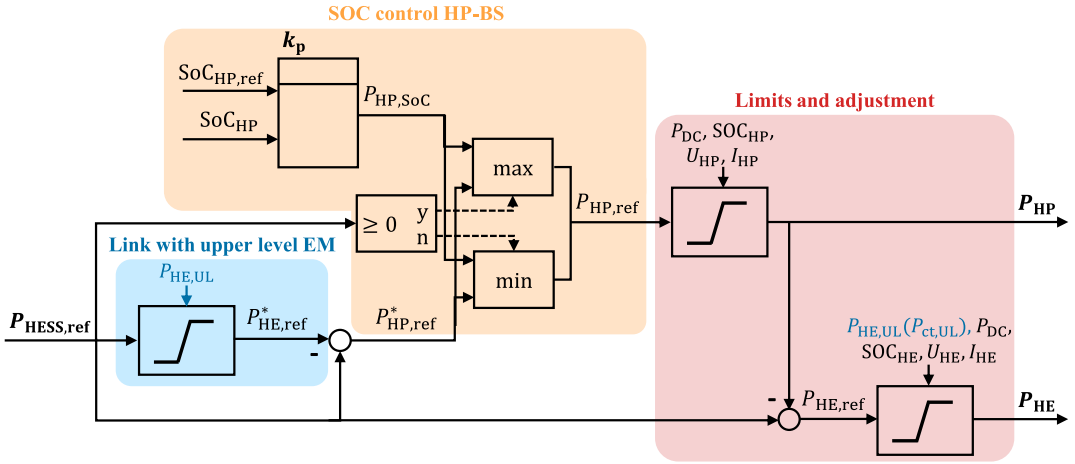

FIGURE 10. Control scheme of lower level EM for power sharing within the HESS.

chosen. For example, a reference SOC of 50 % might be set to be able to absorb power peaks in both directions. However, by predictively determining the $SOC_{HP,ref}$, the required capacity of the HP-BS can theoretically be halved. For this purpose, we adopted the approach of De La Parra et al. [18]. They used the clear-sky envelope of the PV plant power $P_{PV,max}$ (derived from the clear-sky irradiance, see Fig. 3) and 10 % of it as an empirical lower envelope $P_{PV,min}$. From these envelopes, it can be estimated how high the power fluctuations can be in the upward and downward directions. For example, if the current PV power is close to the power output under clear-sky conditions, passing clouds may cause deep power dips, but there may only be small power increases. Consequently, the HP-BS should have a high SOC. At a PV power near the lower envelope, a low SOC is advantageous. Since a multi-use application is considered in this study, $SOC_{HP,ref}$ is not calculated from the forecasted PV power, but from the scheduled grid power in the next interval $P_{g,UL}(k+1)$. The reserves $SOC_{HP,dch}$ and $SOC_{HP,ch}$ to be held for discharging and charging are:

$$SOC_{HP,dch} = (P_{g,UL}(k+1) - \alpha_s \cdot P_{PV,min}(k+1)) \quad (30)$$

$$SOC_{HP,ch} = SOC_{HP,max} - \alpha_s \cdot (P_{PV,max}(k+1) - P_{g,UL}(k+1)). \quad (31)$$

The factor α_s depends on the size of the system; here, $\alpha_s = 9 \times 10^{-7}\ \frac{1}{W}$ was chosen. The reserves $SOC_{HP,dch}$ and $SOC_{HP,ch}$ are further limited to the minimum and maximum SOC of the HP-BS. Then, $SOC_{HP,ref}$ is determined from the two SOC reserves with the following prioritization:

1. The discharge reserve should be available to compensate for drops in power output.
2. The charge reserve should be available to avoid curtailment of PV power.
3. The current SOC_{HP} should be kept to avoid unnecessary energy throughput.

A proportional controller with $\alpha_p = 0.15$ is used to calculate the charge control power $P_{HP,SOC}$:

$$P_{HP,SOC} = (SOC_{HP} - SOC_{HP,ref}) \cdot \frac{E_{HP,nom}}{\Delta t_{LL}} \cdot \alpha_p. \quad (32)$$

Simple lower level EM. We also implemented a simple version of the lower level EM to differentiate between the technical advantages of the HESS (lower total losses and a higher power capability compared to a HE-BS of the same capacity) and the advantages of the developed strategy-based lower level EM. As given in (33) – (35), the simple lower level EM allocates power according to the respective available capacities $Q_{x,ch}$ or $Q_{x,dch}$ in the charging or discharging direction, with x ∈ {HE, HP}. This keeps the SOCs of both the BESSs close to each other.

$$Q_{x,ch} = (SOC_x - SOC_{x,min}) \cdot Q_{x,nom} \cdot SOH_x \quad (33)$$

$$Q_{x,dch} = (SOC_{x,max} - SOC_x) \cdot Q_{x,nom} \cdot SOH_x \quad (34)$$

$$\frac{P_{HE}}{P_{HESS,ch/dch}} = \frac{Q_{HE,ch/dch}}{Q_{HE,ch/dch} + Q_{HP,ch/dch}} \quad (35)$$

Additionally, the HP-BS covers power peaks that exceed the power capability of the HE-BS.

This approach has been found to be advantageous for BESSs with heterogeneous battery modules, whose differing properties are not to be explicitly exploited [71].

IV. PERFORMANCE EVALUATION

The performance of the proposed EM was investigated through comprehensive simulations. We addressed the configuration of the multi-use tasks and hybridization, as well as the contribution of both levels of the EM to maximize the benefit of the battery storage over its lifetime.

A. REDUCING THE SIMULATION TIME

A simulation over the entire lifetime would be very time-consuming for the upper level EM with two-dimensional PWA linearization (2D-MILP). Therefore, we estimate the

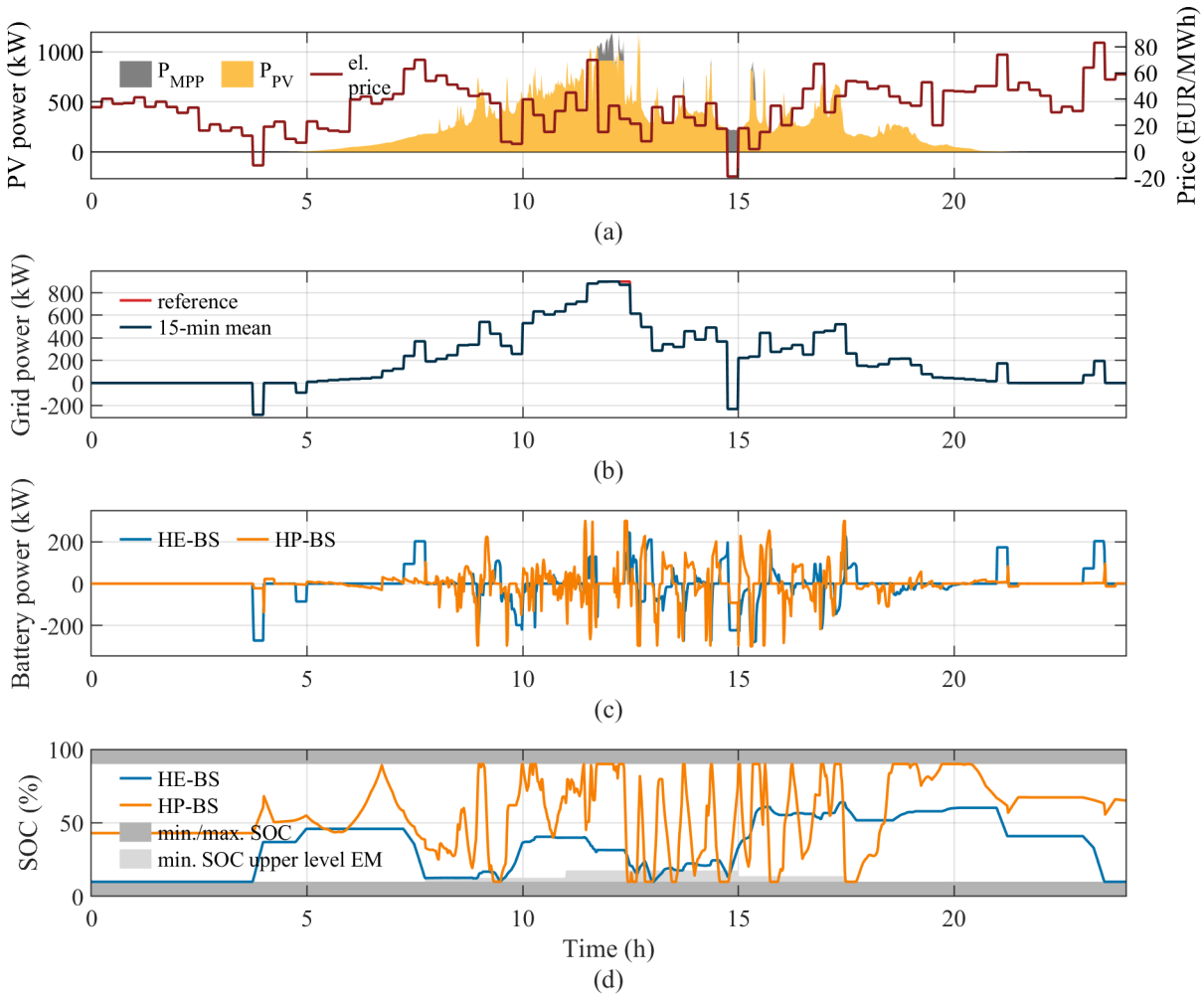

FIGURE 11. Simulation results on a cloudy summer day for Case 1. Deviations between P_{MPP} and P_{PV} indicate curtailment of PV power, whereas deviations between the reference power and the 15-min mean value indicate noncompliance with the settled grid power.

expected lifetimes of the HE-BS from one-year simulations with an initial SOH_{HE} of 90 %. To this end, the resulting time series of the aging stress are repeatedly fed to the battery degradation model until a capacity loss of 20 % is reached.

To assess the error caused by this extrapolation, we compared the HE-BS lifetime resulting from a full-life simulation and the one-year estimate for a less computationally expensive upper level EM, where the PWA linearization is only a function of the battery power (1D-MILP). The extrapolation underestimated the HE-BS lifetime by 1.55 % when using the last price, and by 1.09 % when using the weighted average price.

B. CASE STUDIES

Six cases were designed to investigate the different impacts of the BESS and EM configurations. In Case 1 (base scenario), the HESS consists of two HE-BS modules and two HP-BS modules. The grid power gradient is limited to $\Delta p_g = 20\,\%/\text{min}$ of the maximum grid power of $P_{PCC,max} = 900\,\text{kW}$, and charging the HESS from the grid is allowed. For spot market trading, the last price is used because it has stronger price spreads than the weighted average price (see Fig. 4).

Case 2 and Case 3 address the impact of hybridization. To investigate the improvements owing to intelligent power sharing within the HESS, the simple lower level EM is used in Case 2. In Case 3, both LTO HP-BS modules are replaced with one more LFP HE-BS module, so that the technical differences between the HESS and the single BESS are also represented.

Case 4 investigates the influence of the detailed representation of losses and battery degradation in the 2D-MILP framework by replacing it with a constant conversion efficiency of 95 % and constant average battery degradation costs in the upper level EM.

The purchase of power from the grid is prohibited in Case 5. This eliminates the use case of energy arbitrage, whereas the price differences in the spot market can still be exploited by the energy time shift. Thus, Case 5 illustrates the relevance of multi-use.

To investigate the influence of the price spread at the spot market, we applied the weighted average price instead of the last price in Case 6.

C. QUALITATIVE SIMULATION RESULTS

First, the functionality of the EM is demonstrated for Case 1 on an example day. As can be seen from the PV power profile in Fig. 11a, it is a summer day with highly variable cloud cover and a typical price pattern, with negative prices in two intervals. A deviation of the theoretically possible power P_{MPP} and the actual power output P_{PV} indicates curtailment of the PV power. When prices are negative, there is always full curtailment. If the PV power exceeds the maximum allowed or planned feed-in power, the excess power is either stored or curtailed depending on the battery degradation costs, spot market prices, and technical constraints of the HESS. The 15-min mean grid power values are shown in Fig. 11b. They always match the reference power, except for one interval at midday when the forecast error exceeds the maximum power of the HESS. From the curves of the battery power in Fig. 11c, the desired HESS power sharing can be recognized: The HE-BS covers the energy throughput at moderate power, and the HP-BS covers the power peaks and strong fluctuations resulting from the PV power profile. This characteristic is also reflected in the SOC profiles in Fig. 11d.

To illustrate the long-term influence of both EM levels on the battery aging stress, Fig. 12 shows the frequency of the normalized power and SOC of the HE-BS for Case 1, Case 2 and Case 4. The bins correspond to the segments of the PWA linearization. The influence of the prorated degradation per time step from Fig. 8 can be directly recognized in the histogram of Case 1. High charging and discharging powers, which are associated with high battery losses and degradation costs, are avoided. In addition to that, the SOC shifts downward in the idle state, which minimizes calendar aging.

Fig. 12b shows the results for Case 2, where the simple lower level EM is applied. It is apparent that the HE-BS is significantly less relieved by the HP-BS than in Case 1. First, many rest periods shift to the low power range. In addition to cyclic aging, this is associated with the poor efficiency of the DC/DC converter in the low partial load range. Second, the HE-BS must charge and discharge at a high power more frequently.

At a constant efficiency and battery degradation cost (Case 4 in Fig. 12c), an average SOC is prevalent, and the power is mostly either in the range of the maximum charging or discharging power, or zero. This is to be expected because the battery preferably operates at full power as soon as the revenue exceeds the threshold of the degradation cost and conversion losses.

D. QUANTITATIVE SIMULATION RESULTS

Table 3 presents the results of the techno-economic simulations for the six cases. The upper part of Table 3 shows the results of the one-year simulations with an initial $\mathrm{SOH_{HE}}$ of 90 %, whereas the lower part of Table 3 contains the extrapolated values for the entire HE-BS lifetime. The performance criteria in Table 3 are explained in the following subsection and the results are discussed in IV-D2.

1) PERFORMANCE CRITERIA

We define the BESS profit as the opportunity profit compared to a reference system. This allows for an approximate distinction between the revenue of the PV plant and the additional revenue of each BESS configuration. The reference system consists of the same PV plant, which is equipped with three modules of the HP-BS to limit the gradient of grid power to $\Delta p_{\mathrm{g}} = 20\,\%/\mathrm{min}$. For this purpose, the control strategy proposed in [18] is applied. The grid feed-in of the reference system is remunerated at 94 % of the intraday market price, and no forecast values need to be met. Assuming the last price and the volume-weighted average price, the average annual revenues of the reference system are 62 650 EUR and 62 200 EUR, respectively.

The deviations of the energy exchanged with the grid are given relative to the total exchanged energy, whereas the violations of the grid power gradient are given as absolute incidences, that is, in minutes per year.

After taking these last two criteria into account, the benefit-cost ratio BCR can serve as a metric for the benefit of the BESS over its lifetime and is therefore the central performance criterion. To calculate the benefit-cost ratio, we assume the lifetimes $t_{\mathrm{DC,EOL}}$ of the DC/DC converters and $t_{\mathrm{HP,EOL}}$ of the HP-BS modules to be 15 years. The HE-BS modules are replaced once they have reached their end-of-life, and the reinvestment costs are scaled linearly. The discount factor is set to zero. Perspectively, the battery replacement cost C_{b} could be dynamically adjusted in the EM to reflect the discount factor and integer nature of replacements. However, it would bias the results if they were considered only in the evaluation. The benefit-cost ratio is calculated from the average profit difference per year $\overline{\Delta C_{\mathrm{y}}}$, relative to the total (re)investment costs over the respective lifetimes:

$$\mathrm{BCR} = \frac{\overline{\Delta C_{\mathrm{y}}}}{\frac{\Delta n_{\mathrm{HE}} \cdot C_{\mathrm{HEm}}}{t_{\mathrm{HE,EOL}}} + \frac{(\Delta n_{\mathrm{HE}} + \Delta n_{\mathrm{HP}}) \cdot C_{\mathrm{DCm}}}{t_{\mathrm{DC,EOL}}} + \frac{\Delta n_{\mathrm{HP}} \cdot C_{\mathrm{HPm}}}{t_{\mathrm{HP,EOL}}}}. \quad (36)$$

The parameters C_{HEm} and C_{HPm} are the costs of the HE-BS modules and HP-BS modules, respectively. C_{DCm} is the cost of a DC/DC converter, and $\Delta n_{\mathrm{HE/HP}}$ is the difference in the number of the respective battery modules compared to the reference system.

Again, the EM with 1D-MILP was used to estimate the deviation between the extrapolated benefit-cost ratio from the one-year simulation and the benefit-cost ratio resulting from the full-life simulation. When using the last price for spot market trading, the extrapolation overestimated the benefit-cost ratio by 1.09 %, whereas the extrapolation errors of lifetime and profit difference compensated each other when using the weighted average price.

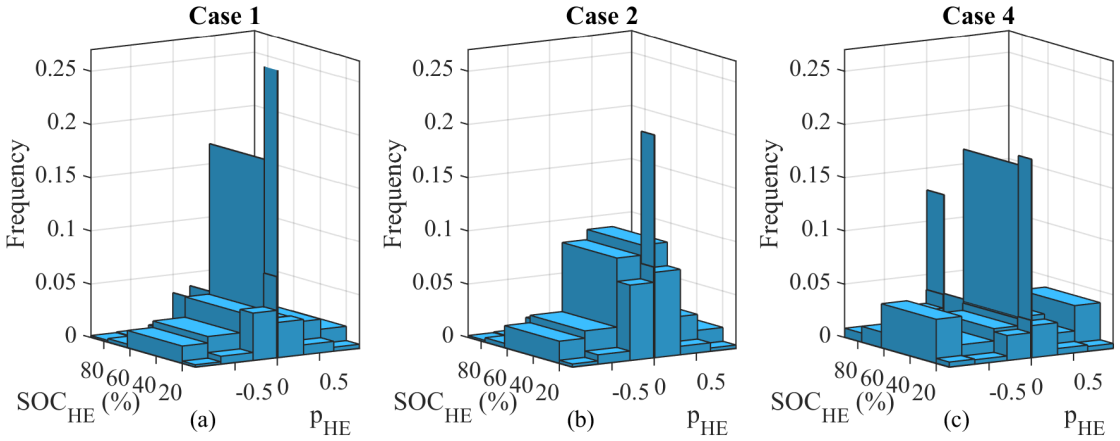

FIGURE 12. Distribution of normalized HE-BS power p_{HE} and SOC_{HE} in one year over the segments of two-dimensional PWA linearization: (a) base scenario (Case 1), (b) 2D-MILP with simple lower level EM (Case 2), and (c) with constant efficiency and battery degradation cost (Case 4).

TABLE 3. Techno-economic results of one-year simulation with an initial SOH of 90 %, and extrapolated values for the entire HE battery lifetime.

	Case 1 base scenario	**Case 2** simple lower level EM	**Case 3** single storage	**Case 4** no PWA linearization	**Case 5** no grid supply	**Case 6** low price variability
Number of BESS modules	2xHE-BS, 2xHP-BS	2xHE-BS, 2xHP-BS	3xHE-BS	2xHE-BS, 2xHP-BS	2xHE-BS, 2xHP-BS	2xHE-BS, 2xHP-BS
Intraday market prices	last price	last price	last price	last price	last price	volume-weighted average price
Profit difference (EUR)	12430	12670	15980	15670	6180	4800
Energy throughput (MWh)	406	389	475	593	270	257
– of which HP-BS (%)	34	15	0	29	46	50
Total storage losses (%)	4.69	5.16	5.15	5.29	4.41	4.37
Deviations of grid energy (%)	0.52	0.53	0.79	1.18	0.53	0.50
Ramp-rate violations	300	390	570	330	320	290
Expected HE-BS lifetime (years)	7.33	6.28	6.60	4.60	11.91	12.29
Proportion of cyclic aging (%)	48.4	52.2	51.5	54.6	40.5	39.1
Benefit-cost ratio BESS	**1.64**	**1.42**	**1.39**	**1.27**	**1.38**	**1.11**

2) DISCUSSION

The slightly higher revenues with lower energy throughput in Case 2 at first seem to speak in favor of the simple lower level EM. However, the throughput has shifted significantly to the detriment of the HE-BS, which shortens its lifetime by more than one year and hence reduces the benefit-cost ratio by more than 13 %. Furthermore, the proposed lower level EM demonstrates advantages in terms of lower total losses and a 30 % lower violation of the grid power gradient. This confirms the effectiveness of the developed charging strategy for the HP-BS. The results for Case 3 illustrate the advantages of hybridization for the configuration in this study; although the larger size of the HE-BS is beneficial for both lifetime and battery losses, the single BESS performs worse than the HESS in both criteria. Lacking the high-power capability of the LTO battery in Case 3, the number of ramp-rate violations increases by 46 % compared to Case 2 and by 90 % compared to Case 1. The benefit-cost ratio is more than 15 % lower than in Case 1. Moreover, the comparison of Case 2 and Case 3 highlights the importance of a smart EM to exploit the technical benefits of HESSs.

Case 4 demonstrates the advantages of the PWA linearization. As already discussed in subsection IV-C, the upper level EM of Case 4 shows an uncompromising behavior, which is reflected quantitatively by higher revenues, but also higher losses and a significantly shorter HE-BS lifetime. Moreover, the poorer representation of battery limitations results in more than twice the deviation from the desired grid power. The benefit-cost ratio is approximately 23 % lower than that of the 2D-MILP.

On the other hand, there are significant differences in the computational complexity. The average computation time per time step of the model predictive control for the 2D-MILP is less than 2 s (on an Intel Core i7-6950X) owing to the efficient implementation, whereas the upper limit for the use case is in the range of a few minutes. Thus, the real-time capability of the developed EM should be guaranteed even at lower computational speeds. When shorter computation times are required, for example for HESS sizing, a tradeoff between accuracy and computational effort can be achieved with the 1D-MILP (one-dimensional PWA linearization of battery degradation costs and conversion efficiency).

In Case 5, prohibiting the grid supply eliminates the possibility of energy arbitrage. Apparently, energy arbitrage contributes approximately half of the revenue in Case 1. Despite the significantly extended lifetime, the benefit-cost ratio of Case 5 is 16 % below that of Case 1 – one advantage of multi-use is that the share of calendar aging is reduced, and therefore, the BESS can be better utilized over its lifetime. Similarly, in Case 6, the lower price spreads of the weighted average price mean that there are fewer opportunities to generate revenue through energy time shift and energy arbitrage. The EM responds to this with more cautious use of the HE-BS, which, as in Case 5, leads to lower losses and a significantly longer lifetime. The HP-BS covers half of the total energy throughput, and the annual throughput of the HE-BS is nearly half that of Case 1. Nevertheless, the benefit-cost ratio in this case is the lowest. The low cyclic aging fraction of less than 40 % indicates that the benefit of the HE-BS in Case 6 could be increased by an expanded multi-use portfolio.

V. CONCLUSION AND OUTLOOK

In a future sustainable energy system, the sufficient and efficient use of energy storage systems will play a central role. Multi-use applications and HESSs with suitable EM concepts contribute to this challenge. This article presents an EM for a hybrid battery storage system deployed for the multi-use application of PV capacity firming, spot market trading, and peak shaving. Therefore, the HESS supports the integration of renewable energies into the grid locally by limiting the grid power ramp-rate and the maximum feed-in, and transregionally by responding to electricity price signals. This is enabled by our implementation of capacity firming, which offers a compromise between limiting the dynamics and providing flexibility. The hierarchical EM approach allows for a combination of different temporal scales and levels of modeling detail. The proposed EM considers the short-term grid power requirements and long-term benefits of the HESS over its lifetime in a robust and computationally efficient manner. The results of extensive simulation-based investigations have demonstrated how both EM levels contribute to these goals. The more accurate representation of nonlinear losses and battery aging in the optimization through two-dimensional PWA linearization is of particular importance. This is because the upper level EM sets the reference grid power and the lower level EM draws upon its pre-optimized power values. It was further shown that the hybridization of two different types of lithium-ion batteries has technical and economic advantages in this configuration – but also that well-designed HESS power sharing is required to exploit them.

Although the benefit-cost ratio defined in (36) is well suited as a performance criterion for comparing the cases examined, it should not be misunderstood as profitability in the economic sense. Due to the simplifying assumptions, the benefit-cost ratio is subject to strong economic uncertainties. This can be improved by a more realistic intraday market model, and by dynamically adjusting the battery replacement costs in the EM to include a discount factor and the integer nature of replacements. Another limitation of this study is the strong reliance on uncertain semi-empirical battery aging models with poor data availability. For practical implementation, a self-learning aging model can be incorporated, and the prorated degradation per time step should be adjusted accordingly. Furthermore, the battery model will be extended by a thermal model and thermal management in order to investigate the interactions between electrical, thermal and aging behavior.

The proposed EM concept can be transferred to other HESSs and multi-use portfolios. Future work will investigate a battery-hydrogen HESS, as well as a large-scale BESS with multiple different strings. To investigate other multi-use portfolios, the hierarchical EM can be easily extended to include additional levels, such as another superordinate level for trading on the day-ahead market, or a subordinate level for considering grid connection requirements at a finer temporal resolution. At each level, alternative EM approaches can be developed and compared. The comparison with methods that differ in their handling of nonlinearities (dynamic programming) and uncertainties (stochastic dynamic programming, reinforcement learning [73]) is particularly interesting.

APPENDIX A
MODELING PARAMETERS

Additional modeling parameters are given in Table 4.

TABLE 4. Modeling parameters.

Description	Symbol	Value
PV module area	A_{PVm}	$1.824\,\mathrm{m}^2$
PV module efficiency	η_{MPP}	0.206
PV module temperature coefficient	$\alpha_{\mathrm{PV,T}}$	$-0.0036\,1/^{\circ}\mathrm{C}$
PV module auxiliary efficiency	$\eta_{\mathrm{PV,aux}}$	0.9
PV plant area	A_{PV}	$23\,347\,\mathrm{m}^2$
Atmospheric pressure for forecast	-	$1 \times 10^5\,\mathrm{Pa}$
Ångström turbidity for forecast	-	0.025
HE-BS minimum/maximum SOC	$\mathrm{SOC}_{\mathrm{HE,min/max}}$	10 %, 90 %
HP-BS minimum/maximum SOC	$\mathrm{SOC}_{\mathrm{HP,min/max}}$	10 %, 90 %
Assumed HE-BS cycle depth for degradation cost calculation	-	25 %
Constant prorated degradation per time step for Case 4	-	$1.65 \times 10^{-5}\,\frac{1}{15\mathrm{min}}$
MILP optimality gap	-	0.1 %

APPENDIX B
TWO-DIMENSIONAL PWA LINEARIZATION

Fig. 13 shows an overview of the workflow described in section III-A2. The two-dimensional PWA linearization is expressed by (37) – (45). To implement these equations, the positions of the vertices $v_{\mathrm{p}}(i,j)$ and $v_{\mathrm{SOC}}(i,j)$, their values $v_{\mathrm{cdegr}}(i,j)$, $v_{\mathrm{CR}}(i,j)$ and $v_{\mathrm{DC,L}}(i,j)$, and the indicator matrices I_0 and I_1 have to be calculated in advance. The indicator matrices are required for logarithmic indexing, which reduces the number of binary variables to $B = \lceil \log_2(2 \cdot N_{\mathrm{P}} \cdot N_{\mathrm{SOC}}) \rceil = 6$ per time step ((44) – (45)). The indicator function returns

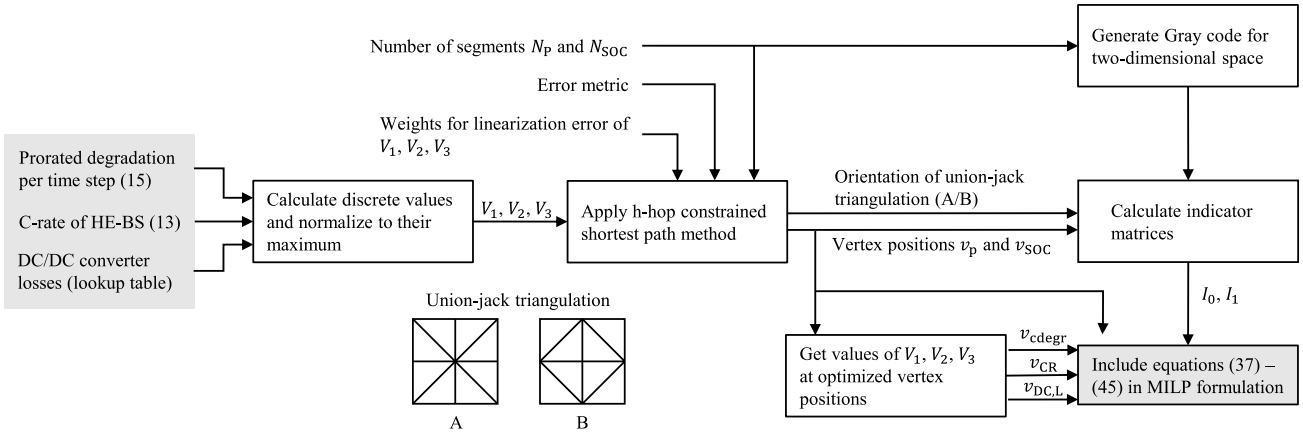

FIGURE 13. Overview of the workflow for two-dimensional PWA linearization using the logarithmic approach with union-jack triangulation.

the value 1 if and only if at a vertex, the Gray codes of all adjacent segments at bit position b take the value 0 (I_0), or take the value 1 (I_1). The resulting indicator matrices are of size $\mathbb{R}^B \times \mathbb{R}^{(N_P+1)} \times \mathbb{R}^{(N_{SOC}+1)}$.

The PWA linearized variables are marked with a tilde. They are calculated as the sum of their vertices $v(i, j)$ weighted with $\lambda(i, j, k)$:

$$\tilde{p}_{HE}(k) = \sum_{i=1}^{N_P+1} \sum_{j=1}^{N_{SOC}+1} \lambda(i,j,k) \cdot v_p(i,j) \tag{37}$$

$$\widetilde{SOC}_{HE}(k) = \sum_{i=1}^{N_P+1} \sum_{j=1}^{N_{SOC}+1} \lambda(i,j,k) \cdot v_{SOC}(i,j) \tag{38}$$

$$\tilde{f}_{degr}(k) = \sum_{i=1}^{N_P+1} \sum_{j=1}^{N_{SOC}+1} \lambda(i,j,k) \cdot v_{cdegr}(i,j) \tag{39}$$

$$\widetilde{CR}_{HE}(k) = \sum_{i=1}^{N_P+1} \sum_{j=1}^{N_{SOC}+1} \lambda(i,j,k) \cdot v_{CR}(i,j) \tag{40}$$

$$\tilde{P}_{DC,L}(k) = \sum_{i=1}^{N_P+1} \sum_{j=1}^{N_{SOC}+1} \lambda(i,j,k) \cdot v_{DC,L}(i,j). \tag{41}$$

The weights are continuous variables in the range of 0 to 1, and add up to 1:

$$0 \leq \lambda(i,j,k) \leq 1 \tag{42}$$

$$\sum_{i=1}^{N_P+1} \sum_{j=1}^{N_{SOC}+1} \lambda(i,j,k) = 1 \tag{43}$$

To ensure that only one segment is active at a time, the binary variables $\delta(b, k) \in \{0, 1\}$ are required, where b is the bit position of the Gray code $b \in \mathbb{Z}$ and $1 \leq b \leq B$:

$$I_0(b,i,j) \cdot \lambda(i,j,k) + \delta(b,k) \leq 1 \quad \forall\, b \tag{44}$$

$$I_1(b,i,j) \cdot \lambda(i,j,k) - \delta(b,k) \leq 0 \quad \forall\, b. \tag{45}$$

For further information, please refer to [33], [38], [39], [40], [68], [69], and [70].

REFERENCES

[1] P. A. Arias et al., "Climate change 2021: The physical science basis. Contribution of working group I to the sixth assessment report of the intergovernmental panel on climate change. Technical summary," in *Proc. Intergovernmental Panel Climate Change*. Cambridge, U.K.: Cambridge Univ. Press, 2021, pp. 33–144, doi: 10.1017/9781009157896.002.

[2] M. Child, O. Koskinen, L. Linnanen, and C. Breyer, "Sustainability guardrails for energy scenarios of the global energy transition," *Renew. Sustain. Energy Rev.*, vol. 91, pp. 321–334, Aug. 2018, doi: 10.1016/j.rser.2018.03.079.

[3] J. Millward-Hopkins, J. K. Steinberger, N. D. Rao, and Y. Oswald, "Providing decent living with minimum energy: A global scenario," *Global Environ. Change*, vol. 65, Nov. 2020, Art. no. 102168, doi: 10.1016/j.gloenvcha.2020.102168.

[4] M. S. Ziegler and J. E. Trancik, "Re-examining rates of lithium-ion battery technology improvement and cost decline," *Energy Environm. Sci.*, vol. 14, no. 4, pp. 1635–1651, Mar. 2021, doi: 10.1039/D0EE02681F.

[5] J. Vetter, P. Novák, M. R. Wagner, C. Veit, K.-C. Möller, J. O. Besenhard, M. Winter, M. Wohlfahrt-Mehrens, C. Vogler, and A. Hammouche, "Ageing mechanisms in lithium-ion batteries," *J. Power Sources*, vol. 147, nos. 1–2, pp. 269–281, Sep. 2005, doi: 10.1016/j.jpowsour.2005.01.006.

[6] X. Han, L. Lu, Y. Zheng, X. Feng, Z. Li, J. Li, and M. Ouyang, "A review on the key issues of the lithium ion battery degradation among the whole life cycle," *eTransportation*, vol. 1, Aug. 2019, Art. no. 100005, doi: 10.1016/j.etran.2019.100005.

[7] N. Kim, N. Shamim, A. Crawford, V. V. Viswanathan, B. M. Sivakumar, Q. Huang, D. Reed, V. Sprenkle, and D. Choi, "Comparison of Li-ion battery chemistries under grid duty cycles," *J. Power Sources*, vol. 546, Oct. 2022, Art. no. 231949, doi: 10.1016/j.jpowsour.2022.231949.

[8] A. Stephan, B. Battke, M. D. Beuse, J. H. Clausdeinken, and T. S. Schmidt, "Limiting the public cost of stationary battery deployment by combining applications," *Nature Energy*, vol. 1, no. 7, pp. 1–9, Jun. 2016, doi: 10.1038/nenergy.2016.79.

[9] S. Englberger, A. Jossen, and H. Hesse, "Unlocking the potential of battery storage with the dynamic stacking of multiple applications," *Cell Rep. Phys. Sci.*, vol. 1, no. 11, Nov. 2020, Art. no. 100238, doi: 10.1016/j.xcrp.2020.100238.

[10] T. Bocklisch, "Hybrid energy storage approach for renewable energy applications," *J. Energy Storage*, vol. 8, no. 1, pp. 311–319, Feb. 2016, doi: 10.1016/j.solener.2013.10.037.

[11] M. Böttiger, M. Wicke, S. Sacht, F. Härtel, R. Gelleschus, and T. Bocklisch, "Hybrid lithium-ion battery storage solution with optimizing energy management and online condition monitoring for multi-use applications," in *Proc. Int. Renew. Energy Storage Conf. (IRES)*. Dordrecht, The Netherlands: Antlantis Press, 2022, pp. 76–92, doi: 10.2991/978-94-6463-156-2_7.

[12] M. Böttiger, M. Paulitschke, R. Beyer, L. Neumann, and T. Bocklisch, "Modular hybrid battery storage system for peak-shaving and self-consumption optimization in industrial applications," *Energy Procedia*, vol. 155, pp. 102–110, Nov. 2018, doi: 10.1016/j.egypro.2018.11.064.

[13] R. Gelleschus, M. Böttiger, and T. Bocklisch, "Optimization-based control concept with feed-in and demand peak shaving for a PV battery heat pump heat storage system," *Energies*, vol. 12, no. 11, p. 2098, Jun. 2019, doi: 10.3390/en12112098.

[14] K. Warner and T. Bocklisch, "Adaptive fuzzy logic controller based energy management for a stand-alone PV hybrid system with battery and hydrogen storage path," in *Proc. Int. Renew. Energy Storage Conf. (IRES)*, 2022, pp. 511–526, doi: 10.2991/978-94-6463-156-2_3.

[15] L. Gerlach and T. Bocklisch, "Experts versus algorithms? Optimized fuzzy logic energy management of autonomous PV hybrid systems with battery and H_2 storage," *Energies*, vol. 14, no. 6, p. 1777, Mar. 2021, doi: 10.3390/en14061777.

[16] E. Bullich-Massagué, F.-J. Cifuentes-García, I. Glenny-Crende, M. Cheah-Mañé, M. Aragüés-Peñalba, F. Díaz-González, and O. Gomis-Bellmunt, "A review of energy storage technologies for large scale photovoltaic power plants," *Appl. Energy*, vol. 274, Sep. 2020, Art. no. 115213, doi: 10.1016/j.apenergy.2020.115213.

[17] J. Martins, S. Spataru, D. Sera, D.-I. Stroe, and A. Lashab, "Comparative study of ramp-rate control algorithms for PV with energy storage systems," *Energies*, vol. 12, no. 7, p. 1342, Apr. 2019, doi: 10.3390/en12071342.

[18] I. de la Parra, J. Marcos, M. García, and L. Marroyo, "Control strategies to use the minimum energy storage requirement for PV power ramp-rate control," *Sol. Energy*, vol. 111, pp. 332–343, Jan. 2015, doi: 10.1016/j.solener.2014.10.038.

[19] A. S. Hintz, K. Rajashekara, and R. Prasanna, "Controller for combined peak-load shaving and capacity firming utilizing multiple energy storage units in a microgrid," in *Proc. IEEE Energy Convers. Congr. Expo. (ECCE)*, Sep. 2016, pp. 1–7, doi: 10.1109/ECCE.2016.7854974.

[20] W. Jiang, L. Zhang, H. Zhao, H. Huang, and R. Hu, "Research on power sharing strategy of hybrid energy storage system in photovoltaic power station based on multi-objective optimisation," *IET Renew. Power Gener.*, vol. 10, no. 5, pp. 575–583, May 2016, doi: 10.1049/iet-rpg.2015.0199.

[21] W. Ma, W. Wang, X. Wu, R. Hu, F. Tang, W. Zhang, X. Han, and L. Ding, "Optimal allocation of hybrid energy storage systems for smoothing photovoltaic power fluctuations considering the active power curtailment of photovoltaic," *IEEE Access*, vol. 7, pp. 74787–74799, 2019, doi: 10.1109/ACCESS.2019.2921316.

[22] V. Miñambres-Marcos, M. Guerrero-Martínez, F. Barrero-González, and M. Milanés-Montero, "A grid connected photovoltaic inverter with battery-supercapacitor hybrid energy storage," *Sensors*, vol. 17, no. 8, p. 1856, Aug. 2017, doi: 10.3390/s17081856.

[23] G. Wang, M. Ciobotaru, and V. G. Agelidis, "Power management for improved dispatch of utility-scale PV plants," *IEEE Trans. Power Syst.*, vol. 31, no. 3, pp. 2297–2306, May 2016, doi: 10.1109/TPWRS.2015.2459065.

[24] *Innovation Landscape Brief: Increasing Time Granularity in Electricity Markets*, Int. Renew. Energy Agency, Abu Dhabi, United Arab Emirates, 2019.

[25] A. Vazquez-Rodriguez, A. Michiorri, and G. Kariniotakis, "Integrating thermal properties and degradation modelling of batteries into the scheduling of hybrid power plants with photovoltaics," *J. Energy Storage*, vol. 73, Dec. 2023, Art. no. 108782, doi: 10.1016/j.est.2023.108782.

[26] A. Saez-de-Ibarra, A. Milo, H. Gaztañaga, V. Debusschere, and S. Bacha, "Co-optimization of storage system sizing and control strategy for intelligent photovoltaic power plants market integration," *IEEE Trans. Sustain. Energy*, vol. 7, no. 4, pp. 1749–1761, Oct. 2016, doi: 10.1109/TSTE.2016.2555704.

[27] I. Hauer, S. Balischewski, and C. Ziegler, "Design and operation strategy for multi-use application of battery energy storage in wind farms," *J. Energy Storage*, vol. 31, Oct. 2020, Art. no. 101572, doi: 10.1016/j.est.2020.101572.

[28] A. Sakti, K. G. Gallagher, N. Sepulveda, C. Uckun, C. Vergara, F. J. de Sisternes, D. W. Dees, and A. Botterud, "Enhanced representations of lithium-ion batteries in power systems models and their effect on the valuation of energy arbitrage applications," *J. Power Sources*, vol. 342, pp. 279–291, Feb. 2017, doi: 10.1016/j.jpowsour.2016.12.063.

[29] B. Xu, J. Zhao, T. Zheng, E. Litvinov, and D. S. Kirschen, "Factoring the cycle aging cost of batteries participating in electricity markets," *IEEE Trans. Power Syst.*, vol. 33, no. 2, pp. 2248–2259, Mar. 2018, doi: 10.1109/TPWRS.2017.2733339.

[30] N. Padmanabhan, M. Ahmed, and K. Bhattacharya, "Battery energy storage systems in energy and reserve markets," *IEEE Trans. Power Syst.*, vol. 35, no. 1, pp. 215–226, Jan. 2020, doi: 10.1109/TPWRS.2019.2936131.

[31] H. Hesse, V. Kumtepeli, M. Schimpe, J. Reniers, D. Howey, A. Tripathi, Y. Wang, and A. Jossen, "Ageing and efficiency aware battery dispatch for arbitrage markets using mixed integer linear programming," *Energies*, vol. 12, no. 6, p. 999, Mar. 2019, doi: 10.3390/en12060999.

[32] R. L. Fares and M. E. Webber, "What are the tradeoffs between battery energy storage cycle life and calendar life in the energy arbitrage application?" *J. Energy Storage*, vol. 16, pp. 37–45, Apr. 2018, doi: 10.1016/j.est.2018.01.002.

[33] V. Kumtepeli, H. C. Hesse, M. Schimpe, A. Tripathi, Y. Wang, and A. Jossen, "Energy arbitrage optimization with battery storage: 3D-MILP for electro-thermal performance and semi-empirical aging models," *IEEE Access*, vol. 8, pp. 204325–204341, 2020, doi: 10.1109/ACCESS.2020.3035504.

[34] M. Schimpe, C. N. Truong, M. Naumann, A. Jossen, H. C. Hesse, J. M. Reniers, and D. A. Howey, "Marginal costs of battery system operation in energy arbitrage based on energy losses and cell degradation," in *Proc. IEEE Int. Conf. Environ. Electr. Eng. IEEE Ind. Commercial Power Syst. Eur. (EEEIC/I&CPS Europe)*, Piscataway, NJ, USA, Jun. 2018, pp. 1–5.

[35] N. Collath, B. Tepe, S. Englberger, A. Jossen, and H. Hesse, "Aging aware operation of lithium-ion battery energy storage systems: A review," *J. Energy Storage*, vol. 55, Nov. 2022, Art. no. 105634, doi: 10.1016/j.est.2022.105634.

[36] A. V. Vykhodtsev, D. Jang, Q. Wang, W. Rosehart, and H. Zareipour, "A review of modelling approaches to characterize lithium-ion battery energy storage systems in techno-economic analyses of power systems," *Renew. Sustain. Energy Rev.*, vol. 166, Sep. 2022, Art. no. 112584, doi: 10.1016/j.rser.2022.112584.

[37] R. Gelleschus and T. Bocklisch, "Impact of model and forecast uncertainties on the performance of the model predictive control of a PV-battery-heat pump-heat storage system," in *Proc. Int. Renew. Energy Storage Conf. (IRES)*, 2022, pp. 162–192, doi: 10.2991/978-94-6463-156-2_13.

[38] J. P. Vielma, S. Ahmed, and G. Nemhauser, "Mixed-integer models for nonseparable piecewise-linear optimization: Unifying framework and extensions," *Oper. Res.*, vol. 58, no. 2, pp. 303–315, Apr. 2010, doi: 10.1287/opre.1090.0721.

[39] J. Huchette and J. P. Vielma, "Nonconvex piecewise linear functions: Advanced formulations and simple modeling tools," 2017, *arXiv:1708.00050*.

[40] J. P. Vielma, "Embedding formulations and complexity for unions of polyhedra," *Manage. Sci.*, vol. 64, no. 10, pp. 4721–4734, Oct. 2018, doi: 10.1287/mnsc.2017.2856.

[41] Y. Yang, S. Bremner, C. Menictas, and M. Kay, "Modelling and optimal energy management for battery energy storage systems in renewable energy systems: A review," *Renew. Sustain. Energy Rev.*, vol. 167, Oct. 2022, Art. no. 112671, doi: 10.1016/j.rser.2022.112671.

[42] C. Ju, P. Wang, L. Goel, and Y. Xu, "A two-layer energy management system for microgrids with hybrid energy storage considering degradation costs," *IEEE Trans. Smart Grid*, vol. 9, no. 6, pp. 6047–6057, Nov. 2018, doi: 10.1109/TSG.2017.2703126.

[43] G. Xu, C. Shang, S. Fan, X. Hu, and H. Cheng, "A hierarchical energy scheduling framework of microgrids with hybrid energy storage systems," *IEEE Access*, vol. 6, pp. 2472–2483, 2018, doi: 10.1109/ACCESS.2017.2783903.

[44] Y. Shi, B. Xu, D. Wang, and B. Zhang, "Using battery storage for peak shaving and frequency regulation: Joint optimization for superlinear gains," *IEEE Trans. Power Syst.*, vol. 33, no. 3, pp. 2882–2894, May 2018, doi: 10.1109/TPWRS.2017.2749512.

[45] H. Su, D. Feng, Y. Zhao, Y. Zhou, Q. Zhou, C. Fang, and U. Rahman, "Optimization of customer-side battery storage for multiple service provision: Arbitrage, peak shaving, and regulation," *IEEE Trans. Ind. Appl.*, vol. 58, no. 2, pp. 2559–2573, Mar. 2022, doi: 10.1109/TIA.2022.3145330.

[46] S. Wacker, "Basic and other measurements of radiation at station Lindenberg," in *Meteorologisches Observatorium Lindenberg*. Tauche, Germany: Deutscher Wetterdienst, 2018, doi: 10.1594/PANGAEA.669521.

[47] V. Quaschning, "Solar radiation," in *Understanding Renewable Energy Systems*. Sterling, VA, USA: Earthscan, 2005, pp. 52–66.

[48] R. Perez, P. Ineichen, R. Seals, J. Michalsky, and R. Stewart, "Modeling daylight availability and irradiance components from direct and global irradiance," *Sol. Energy*, vol. 44, no. 5, pp. 271–289, 1990, doi: 10.1016/0038-092x(90)90055-h.

[49] J. Marcos, L. Marroyo, E. Lorenzo, D. Alvira, and E. Izco, "From irradiance to output power fluctuations: The PV plant as a low pass filter," *Prog. Photovoltaics, Res. Appl.*, vol. 19, no. 5, pp. 505–510, Jan. 2011, doi: 10.1002/pip.1063.
[50] J. Bergner, J. Weniger, T. Tjaden, and V. Quaschning, "Feed-in power limitation of grid-connected PV battery systems with autonomous forecast-based operation strategies," in *Proc. 29th Eur. Photovoltaic Sol. Energy Conf. Exhib.*, Amsterdam, The Netherlands, Sep. 2014, pp. 22–26.
[51] B. E. Psiloglou and H. D. Kambezidis, "Performance of the meteorological radiation model during the solar eclipse of 29 March 2006," *Atmos. Chem. Phys.*, vol. 7, no. 23, pp. 6047–6059, Dec. 2007, doi: 10.5194/acp-7-6047-2007.
[52] EPEX SPOT. *EPEX Intraday Market Data*. Accessed: Jan. 14, 2022. [Online]. Available: https://www.epexspot.com/en/market-data
[53] Tennet. *Balance Group Deviation*. Accessed: Jan. 14, 2022. [Online]. Available: https://www.tennet.eu/electricity-market/german-market/balance-groups/prices-for-balancing-energy/balance-group-deviation/
[54] *HYBAT Research Project*, document 03EI3009C, Fraunhofer Institute for Solar Energy Systems (ISE), Freiburg, Germany, 2023.
[55] EVE Energy. (2021). *Product Specification*. Accessed: Feb. 12, 2024. [Online]. Available: https://www.evebattery-germany.de/wp-content/uploads/2021/02/LF1053.2V-105AhProduct-SpecificationVersion-F-2019.12.02.pdf.
[56] T. Nemeth, P. Schröer, M. Kuipers, and D. U. Sauer, "Lithium titanate oxide battery cells for high-power automotive applications—Electro-thermal properties, aging behavior and cost considerations," *J. Energy Storage*, vol. 31, no. 5, Jul. 2020, Art. no. 101656, doi: 10.1016/j.est.2020.101656.
[57] C. P. Sandhya, B. John, and C. Gouri, "Lithium titanate as anode material for lithium-ion cells: A review," *Ionics*, vol. 20, no. 5, pp. 601–620, Apr. 2014, doi: 10.1007/s11581-014-1113-4.
[58] P. Gasper, K. Gering, E. Dufek, and K. Smith, "Challenging practices of algebraic battery life models through statistical validation and model identification via machine-learning," *J. Electrochem. Soc.*, vol. 168, no. 2, Feb. 2021, Art. no. 020502, doi: 10.1149/1945-7111/abdde1.
[59] M. Naumann, M. Schimpe, P. Keil, H. C. Hesse, and A. Jossen, "Analysis and modeling of calendar aging of a commercial $LiFePO_4$/graphite cell," *J. Energy Storage*, vol. 17, pp. 153–169, Jun. 2018, doi: 10.1016/j.est.2018.01.019.
[60] M. Naumann, F. B. Spingler, and A. Jossen, "Analysis and modeling of cycle aging of a commercial $LiFePO_4$/graphite cell," *J. Power Sources*, vol. 451, Mar. 2020, Art. no. 227666, doi: 10.1016/j.jpowsour.2019.227666.
[61] P. M. Attia, A. Bills, F. B. Planella, P. Dechent, G. dos Reis, M. Dubarry, P. Gasper, R. Gilchrist, S. Greenbank, D. Howey, O. Liu, E. Khoo, Y. Preger, A. Soni, S. Sripad, A. G. Stefanopoulou, and V. Sulzer, "Review—'Knees' in lithium-ion battery aging trajectories," *J. Electrochem. Soc.*, vol. 169, no. 6, Jun. 2022, Art. no. 060517, doi: 10.1149/1945-7111/ac6d13.
[62] Gurobi Optimization Inc. (2022). *Gurobi Optimizer Reference Manual*. Accessed: Nov. 11, 2022. [Online]. Available: http://www.gurobi.com
[63] F. Wankmüller, P. R. Thimmapuram, K. G. Gallagher, and A. Botterud, "Impact of battery degradation on energy arbitrage revenue of grid-level energy storage," *J. Energy Storage*, vol. 10, pp. 56–66, Apr. 2017, doi: 10.1016/j.est.2016.12.004.
[64] G. He, Q. Chen, P. Moutis, S. Kar, and J. F. Whitacre, "An intertemporal decision framework for electrochemical energy storage management," *Nature Energy*, vol. 3, no. 5, pp. 404–412, Apr. 2018, doi: 10.1038/s41560-018-0129-9.
[65] K. Abdulla, J. de Hoog, V. Muenzel, F. Suits, K. Steer, A. Wirth, and S. Halgamuge, "Optimal operation of energy storage systems considering forecasts and battery degradation," *IEEE Trans. Smart Grid*, vol. 9, no. 3, pp. 2086–2096, May 2018, doi: 10.1109/TSG.2016.2606490.
[66] N. Collath, M. Cornejo, V. Engwerth, H. Hesse, and A. Jossen, "Increasing the lifetime profitability of battery energy storage systems through aging aware operation," *Appl. Energy*, vol. 348, Oct. 2023, Art. no. 121531, doi: 10.1016/j.apenergy.2023.121531.
[67] A. Karger, L. Wildfeuer, D. Aygül, A. Maheshwari, J. P. Singer, and A. Jossen, "Modeling capacity fade of lithium-ion batteries during dynamic cycling considering path dependence," *J. Energy Storage*, vol. 52, Aug. 2022, Art. no. 104718, doi: 10.1016/j.est.2022.104718.
[68] R. Misener and C. A. Floudas, "Piecewise-linear approximations of multidimensional functions," *J. Optim. Theory Appl.*, vol. 145, no. 1, pp. 120–147, Apr. 2010, doi: 10.1007/s10957-009-9626-0.
[69] F. Gray, "Pulse code communication," U.S. Patent 2 632 058, Mar. 17, 1953.
[70] V. Vasudeva, "Global optimization with piecewise linear approximation," Ph.D. dissertation, Dept. Inf., Risk, Oper. Manag. (IROM), Univ. Texas, Austin, TX, USA, 2015.
[71] M. Bauer, M. Muehlbauer, O. Bohlen, M. A. Danzer, and J. Lygeros, "Power flow in heterogeneous battery systems," *J. Energy Storage*, vol. 25, Oct. 2019, Art. no. 100816, doi: 10.1016/j.est.2019.100816.
[72] R. Wegmann, V. Döge, and D. U. Sauer, "Assessing the potential of a hybrid battery system to reduce battery aging in an electric vehicle by studying the cycle life of a graphite|NCA high energy and a LTO|metal oxide high power battery cell considering realistic test profiles," *Appl. Energy*, vol. 226, pp. 197–212, Sep. 2018, doi: 10.1016/j.apenergy.2018.05.104.
[73] F. Härtel and T. Bocklisch, "Minimizing energy cost in PV battery storage systems using reinforcement learning," *IEEE Access*, vol. 11, pp. 39855–39865, 2023, doi: 10.1109/ACCESS.2023.3267978.

MARGRIT WICKE received the Dipl.-Ing. degree in renewable energy systems from Dresden University of Technology, Germany, in 2021.

During her graduate studies, she was a Research and Development Intern with Belectric Solar and Battery GmbH. She is currently a Research Associate with the Chair of Energy Storage Systems, Dresden University of Technology. Her research interests include energy management of renewable energy storage systems, control and applications of hybrid energy storage systems, and lithium-ion battery aging. She was awarded the Franz Stolze Prize for her Diploma Thesis in 2022.

THILO BOCKLISCH received the Dipl.-Ing. and Ph.D. degrees in electrical engineering from Chemnitz University of Technology, Germany, in 2003 and 2009, respectively.

From 2003 to 2008, he was a Research Assistant with the Chair of Electrical Machines and Drives, Chemnitz University of Technology. From 2008 to 2013, he was the Head of the Interdisciplinary Research Group "Intelligent Decentralized Energy Storage Systems" and the Research Group "Multi-Storage Hybrid Systems" with the Chair of Power Systems and High-Voltage Engineering, Chemnitz University of Technology, from 2009 to 2016. In 2016, he was appointed an University Professor and the Head of the Chair of Energy Storage Systems, Dresden University of Technology. He is the author of more than 50 scientific articles. His research interests include design, modeling, control and applications of hybrid energy storage systems, modeling, simulation and optimization of energy storage and energy conversion devices, sustainable energy supply concepts for power, heat and transport including sector coupling, prediction, and classification of energy time series. He received the Dresdner Gesprächskreis der Wirtschaft und der Wissenschaft e.V. Award for outstanding results in the Ph.D. thesis, in 2011. He is currently the Chairperson of the Annual Energy Storage Symposium, Dresden University of Technology.